

REGENERATED AMORPHOUS CELLULOSE FROM  
PINEAPPLE LEAF FIBERS VIA SULFURIC ACID  
TREATMENT

Miss Gisma Coraima Asmarani



A Thesis Submitted in Partial Fulfillment of the Requirements  
for the Degree of Master of Science in Chemistry  
Department of Chemistry  
FACULTY OF SCIENCE  
Chulalongkorn University  
Academic Year 2020  
Copyright of Chulalongkorn University

เชลลูโลสอสัณฐานสร้างใหม่จากเส้นใยใบสับประรดผ่านการบำบัดด้วยกรดกำมะถัน



น.ส.กีสมา โคโรมา อัสมารานี

วิทยานิพนธ์นี้เป็นส่วนหนึ่งของการศึกษาตามหลักสูตรปริญญาวิทยาศาสตรมหาบัณฑิต

สาขาวิชาเคมี ภาควิชาเคมี

คณะวิทยาศาสตร์ จุฬาลงกรณ์มหาวิทยาลัย

ปีการศึกษา 2563

ลิขสิทธิ์ของจุฬาลงกรณ์มหาวิทยาลัย



กีสมา โควโรมา อัสมารานี : เซลลูโลสอสัณฐานสร้างใหม่จากเส้นใยใบสับประรดผ่านการบำบัดด้วยกรดกำมะถัน.  
 ( REGENERATED AMORPHOUS CELLULOSE FROM PINEAPPLE  
 LEAF FIBERS VIA SULFURIC ACID TREATMENT ) อ.ที่ปรึกษาหลัก : ศ. ดร.  
 สอนง เอกสิทธิ์

เส้นใยจากใบสับประรดเป็นวัสดุเหลือใช้ทางการเกษตรที่มีอยู่มากมายในประเทศไทย ที่สามารถนำกลับมาใช้ใหม่ได้เนื่องจากมีปริมาณเซลลูโลสสูง งานวิจัยนี้ได้พัฒนากระบวนการอย่างง่ายโดยใช้กรดซัลฟิวริกเพื่อผลิตผลิตภัณฑ์เซลลูโลส 3 ชนิดจากเส้นใยจากใบสับประรด ได้แก่ เซลลูโลสที่ผลิตขึ้นใหม่อย่างออสัณฐาน (RAC), ฟลิกไมโครเซลลูโลส (MCC), และฟลิกนาโนเซลลูโลส (NCC) กระบวนการใช้กรดซัลฟิวริกนี้ดำเนินการที่ความเข้มข้น 25% และ 50% โดยปริมาตรที่อุณหภูมิแตกต่างกัน 3 อุณหภูมิ (-20, 30 และ 50 องศาเซลเซียส) ในสภาวะที่ความเข้มข้นกรดซัลฟิวริก 25% โดยปริมาตร สามารถใช้ผลิตฟลิกไมโครเซลลูโลสที่มีความยาวแตกต่างกันได้ (ประมาณ  $29.57 \pm 9.99$  ถึง  $106.40 \pm 61.10 \mu\text{m}$ ) โดยขึ้นอยู่กับอุณหภูมิที่ใช้ การควบคุมสภาวะของอุณหภูมิที่แตกต่างกันนี้จะสามารถควบคุมขนาดของฟลิกไมโครเซลลูโลสได้โดยไม่ทำให้โครงสร้างทางเคมีเปลี่ยนแปลง โดยยืนยันจากภาพจากกล้องจุลทรรศน์และสเปกตรัม FT-IR เมื่อเปรียบเทียบกับฟลิกไมโครเซลลูโลสจากผลิตภัณฑ์เชิงพาณิชย์ Avicel PH101 ฟลิกไมโครเซลลูโลสที่ผลิตได้มีข้อได้เปรียบเหนือ Avicel PH101 ในด้านสัดส่วนและขนาดสม่ำเสมอ ฟลิกไมโครเซลลูโลสที่ผลิตได้ในสภาวะนี้มีจึงศักยภาพในการเป็นทางเลือกหนึ่งในการผลิตฟลิกไมโครเซลลูโลสเชิงพาณิชย์ได้ ในสภาวะที่ความเข้มข้นกรดซัลฟิวริก 50% โดยปริมาตร สามารถใช้ผลิตผลิตภัณฑ์เซลลูโลสได้ถึง 3 ชนิด โดยสามารถจำแนกได้จากกล้องจุลทรรศน์, cross-polarizer, FT-IR และ XRD เมื่อผลิตที่อุณหภูมิ -20 องศาเซลเซียส จะได้ผลิตภัณฑ์เป็นเซลลูโลสที่ผลิตขึ้นใหม่อย่างออสัณฐานโดยยืนยันจากลักษณะสัมพัทธ์สลายเจล, ไม่มีปรากฏการณ์เชิงแสงไบรีฟริงเจนซ์ การหายไปของแถบฟลิกบนสเปกตรัม FT-IR บริเวณตำแหน่งยอดที่  $1425 \text{ cm}^{-1}$  และการดูดกลืนแสงที่เพิ่มขึ้นของแถบออสัณฐานบนสเปกตรัม FT-IR ที่ตำแหน่งยอดบริเวณ  $897 \text{ cm}^{-1}$ , และรูปแบบ XRD ที่สอดคล้องกับเซลลูโลส II ซึ่งมีลักษณะออสัณฐาน เมื่อผลิตที่อุณหภูมิ 30 องศาเซลเซียสจะได้ผลิตภัณฑ์เป็นฟลิกไมโครเซลลูโลส ภาพจากกล้องจุลทรรศน์แสดงให้เห็นรูปร่างรวมถึงความยาวและความกว้างของเส้นใยที่  $37.63 \pm 14.19$  และ  $3.85 \pm 0.66 \mu\text{m}$  ตามลำดับ ในขณะที่อุณหภูมิ 50 องศาเซลเซียสได้ผลิตภัณฑ์เป็นฟลิกนาโนเซลลูโลส ซึ่งสังเกตได้จากปรากฏการณ์เชิงแสงไบรีฟริงเจนซ์ภายใต้ cross-polarizer ดังนั้นการผลิตเซลลูโลสที่ผลิตขึ้นใหม่อย่างออสัณฐานหรือฟลิกนาโนเซลลูโลสจำเป็นต้องใช้กรดที่มีความเข้มข้นสูงพอควบคู่กับการใช้อุณหภูมิที่เหมาะสม การปรับอุณหภูมิในความเข้มข้นที่เหมาะสมยังให้ผลิตภัณฑ์ที่แตกต่างกันอีกด้วย

CHULALONGKORN UNIVERSITY

สาขาวิชา เคมี  
 ปีการศึกษา 2563

ลายมือชื่อนิติศ .....  
 ลายมือชื่อ อ.ที่ปรึกษาหลัก .....

# # 6171915723 : MAJOR CHEMISTRY

KEYWORD Pineapple leaf fiber, Regenerated amorphous cellulose, sulfuric acid  
D:

Gisma Coraima Asmarani : REGENERATED AMORPHOUS  
CELLULOSE FROM PINEAPPLE LEAF FIBERS VIA SULFURIC  
ACID TREATMENT . Advisor: Prof. SANONG EKGASIT, Ph.D.

Pineapple leaf fiber (PALF) is an agricultural residue available abundantly in Thailand as a renewable resource with high cellulose content. In this research, a simple process using sulfuric acid ( $\text{H}_2\text{SO}_4$ ) treatment has been developed to produce three types of cellulosic products from PALF, which are regenerated amorphous (RAC), microcrystalline (MCC), and nanocrystalline (NCC) cellulose.  $\text{H}_2\text{SO}_4$  acid treatment has been done in 25% and 50% (v/v)  $\text{H}_2\text{SO}_4$  under three different temperatures (-20, 30, and 50 °C). In 25% (v/v)  $\text{H}_2\text{SO}_4$ , various MCC lengths (about  $29.57 \pm 9.99$  to  $106.40 \pm 61.10$   $\mu\text{m}$ ) were produced from different temperatures. Different temperatures in this condition gave the ability to control the MCC size without changing the chemical structure, confirmed by OM images and FT-IR spectra. Compared to the commercial MCC, Avicel PH101, MCC PALF obtained in this work offers definite advantages over Avicel PH101 regarding aspect ratio and uniformity. MCC PALF can be a potential alternative to produce a commercial MCC. In 50% (v/v)  $\text{H}_2\text{SO}_4$ , three kinds of cellulosic products were obtained and could be differentiated using OM, cross-polarizer, FT-IR, and XRD characterizations. RAC was obtained at -20 °C, confirmed from the gel-like shape morphology, no birefringence shown, the crystalline band's disappearance at  $1425\text{ cm}^{-1}$  and increment of the amorphous band at  $897\text{ cm}^{-1}$  on FT-IR spectrum, and XRD patterns of amorphous cellulose with small peaks corresponding to cellulose II. MCC was obtained at 30 °C, showing a short fiber morphology in OM image with length and width at  $37.63 \pm 14.19$  and  $3.85 \pm 0.66$   $\mu\text{m}$ , respectively. NCC was obtained at 50 °C, showing flow birefringence phenomena, confirmed by cross-polarizer. Producing RAC and NCC required adequate acid concentration and temperature treatment. By adjusting the temperature in an appropriate concentration, different products could be obtained.

Field of Study: Chemistry

Student's Signature

Academic Year: 2020

Advisor's Signature

Year:

.....

## ACKNOWLEDGEMENTS

First and foremost, praises and thanks to God, the Almighty, for His showers of blessings throughout my research.

I would like to express my deep and sincere gratitude to my thesis advisor, Professor Dr. Sanong Ekgasit, for providing the support, suggestions, motivation, training, and understanding, as well as patiently practices my technical skill during the whole research. I am extending my heartfelt thanks to Assoc. Prof. Dr. Kanet Wongravee and Asst. Prof. Dr. Prompong Pienpinijtham for always give so much positive advice and motivation to my research.

Special thanks are also given to Dr. Attasith Parnsubsakul and Dr. Umphan Ngoensawat. I appreciate the generous contribution, kindness, encouragement, and sound advice throughout my research training.

I would like to show my appreciation to my thesis committee: Assoc. Prof. Dr. Vudichai Parasuk, Assoc. Prof. Voravee Hoven, and Asst. Prof. Dr. Warunee Ariyawiriyanan for their insightful suggestions and encouragement.

I would like to sincerely thank my colleagues in Sensor Research Unit (SRU), Chulalongkorn University, and all good friends here for suggestions and supports throughout my graduate study.

Besides, I gratefully acknowledge the ASEAN Scholarship Chulalongkorn University for my scholarship and financial support.

Last but not least, I am proudly grateful to my family, fiancée, and friends far from my homeland for their unconditional love, supports, and encouragement all this time.

Gisma Coraima Asmarani

## TABLE OF CONTENTS

	<b>Page</b>
ABSTRACT (THAI) .....	iii
ABSTRACT (ENGLISH).....	iv
ACKNOWLEDGEMENTS .....	v
TABLE OF CONTENTS.....	vi
CHAPTER I INTRODUCTION.....	7
1.1 Research background.....	7
1.2 The objectives.....	9
1.3 The scopes of research.....	9
CHAPTER II THEORETICAL BACKGROUND.....	10
2.1 Pineapple leaf fiber (PALF) .....	10
2.1.1 Cellulose content in PALF compared with other agricultural wastes.....	10
2.1.2 Purification in PALF .....	11
2.1.2.1 Major impurities in PALF .....	11
2.1.2.2 Advantages and disadvantages of purification treatment .....	12
2.2 Cellulose .....	14
2.2.1 Cellulose structure.....	14
2.2.2 Cellulosic products .....	15
2.2.2.1 Microcrystalline cellulose (MCC) .....	15
2.2.2.2 Nanocrystalline cellulose (NCC).....	16
2.2.2.3 Nanofibril cellulose (NFC).....	17
2.2.2.4 Regenerated amorphous cellulose (RAC) .....	18
2.3 Methods to obtain RAC.....	19
2.3.1 N-methylmorpholine-N-oxide (NMMO) .....	19
2.3.2 Inorganic salts.....	19
2.3.3 Ionic liquids (IL) .....	20

2.3.4 NaOH/Urea.....	20
2.3.5 LiCl/N,N-dimethylacetamide (LiCl/DMAc).....	21
2.3.6 Acid treatment .....	21
2.4 Applications of RAC .....	22
CHAPTER III EXPERIMENTAL SECTION.....	24
3.1 Chemical reagents .....	24
3.2 Instruments .....	24
3.3 Purification of raw PALF .....	25
3.3.1 PALF pretreatment.....	25
3.3.2 Alkali treatment.....	25
3.3.3 Bleaching treatment.....	25
3.4 Preparation of cellulosic products from bleached PALF via sulfuric acid treatment.....	26
3.5 Characterizations .....	27
3.5.1 Optical microscopy (OM) .....	27
3.5.2 Fourier-transform infrared (FT-IR) spectroscopy .....	27
3.5.3 Birefringence analysis .....	28
3.5.4 Thermal gravimetric analysis (TGA) .....	28
3.5.5 X-ray Diffraction (XRD).....	28
CHAPTER IV .....	29
RESULTS AND DISCUSSION .....	29
4.1 Purification of pineapple leaf fiber (PALF) .....	29
4.1.1 Physical changes in PALF after purification treatment.....	29
4.1.2 Chemical structural changes in PALF after purification treatment.....	33
4.1.3 Comparison of bleached PALF with commercial cellulose standards.....	36
4.1.4 Thermal properties of PALF .....	39
4.2 PALF in 25% H <sub>2</sub> SO <sub>4</sub> (sulfuric acid) treatment.....	40
4.2.1 Physical properties of PALF after 25% (v/v) sulfuric acid treatment.....	41
4.2.2 Chemical structural changes of PALF in 25% (v/v) H <sub>2</sub> SO <sub>4</sub> .....	46

4.2.3 Thermal properties of bleached PALF and cellulosic products .....	47
4.3 PALF in sulfuric acid treatment of 50% (v/v) H <sub>2</sub> SO <sub>4</sub> .....	49
4.3.1 Physical properties of PALF in 50% (v/v) H <sub>2</sub> SO <sub>4</sub> .....	49
4.3.2 Chemical structural changes of PALF in 50% (v/v) H <sub>2</sub> SO <sub>4</sub> .....	54
4.3.3 X-ray diffraction patterns of bleached PALF and its cellulosic products	58
4.3.4 Thermal properties of bleached PALF and cellulosic products .....	60
CHAPTER V CONCLUSIONS .....	62
REFERENCES .....	63
VITA.....	77



## LIST OF TABLES

Table 2.1 Cellulose content in agricultural wastes.....	11
Table 2.2 Advantages and disadvantages in purification treatment.....	13
Table 2.3 Summary of work using NMMO.....	19
Table 2.4 Summary of work using inorganic salts.....	19
Table 2.5 Summary of works using IL.....	20
Table 2.6 Summary of works using NaOH/Urea.....	21
Table 2.7 Summary of work using LiCl/DMAc.....	21
Table 2.8 Summary of work using the acid treatment.....	22
Table 4.1 Band assignments of FT-IR spectra raw, alkali-treated, and bleached PALF. .....	34
Table 4.2 Band assignments of FT-IR spectra from bleached PALF and BC.....	37
Table 4.3 Thermal properties profiles of raw PALF, alkali-treated PALF, and bleached PALF.....	39
Table 4.4 Average diameter (D), length (L), and aspect ratio (L/D) of bleached PALF, short fibers after sulfuric acid treatment, and Avicel PH101.....	43
Table 4.5 Thermal properties profile of bleached PALF, -20PALF25%, 30PALF25%, and 50PALF25%.....	47
Table 4.6 Band assignment of FT-IR spectra from bleached PALF, -20PALF50%, 30PALF50%, 50PALF50%.....	56
Table 4.7 Corresponding peaks of XRD patterns and crystallinity index (CI).....	58
Table 4.8 Thermal properties profile of bleached PALF, -20PALF50%, 30PALF50%, and 50PALF50%.....	60

## LIST OF FIGURES

Figure 2.1	Production of pineapple leaf fiber, sequential (A) pineapple plant, (B) extraction of fiber from pineapple leaves, and (C) pineapple leaf fiber. Copyright 2015 Hindawi Publishing Corporation. ....	10
Figure 2.2	Chemical structure of lignin.....	11
Figure 2.3	Chemical structure of hemicellulose.....	12
Figure 2.4	Structure of cellulose and its inter and intramolecular H-bonding. ....	14
Figure 2.5	Crystalline and amorphous (disordered) regions in cellulose. Copyright 2011 The Royal Society of Chemistry.....	15
Figure 2.6	Morphology of MCC in SEM images. Copyright 2014 Elsevier Ltd. ....	15
Figure 2.7	Morphology of NCC shown in the TEM image. Copyright 2016 The Royal Society of Chemistry. ....	16
Figure 2.8	Morphology of NFC displayed in the TEM image. Copyright 2018 WILEY-VCH Verlag GmbH & Co. KGaA.....	17
Figure 2.9	Morphology of RAC showed in the SEM image. Copyright 2019 American Chemical Society. ....	18
Figure 2.10	Morphology and microstructure of the CNT-cellulose composite films regenerated from NaOH-Urea aqueous solution: (a) photograph, (b) AFM image, and (c) TEM image. Copyright 2013 The Royal Society of Chemistry.....	23
Figure 2.11	The image of a transparent film of CF11 6%. Copyright 2015 The Royal Society of Chemistry.....	23
Figure 3.1	Purification of PALF using alkali and bleaching treatments.....	25
Figure 3.2	Sulfuric acid treatment of PALF in (A) 25% and (B) 50% (v/v) H <sub>2</sub> SO <sub>4</sub> .....	26

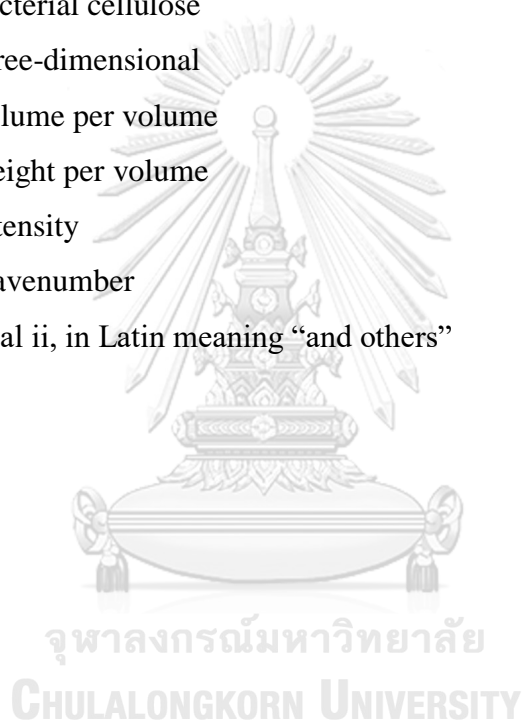
Figure 4.1	(A) Photographic image and (B-D) OM images of raw PALF, (E) drawing illustration of composite-like structure between cellulose, lignin, and hemicellulose in PALF, (F) lignin structure, and (G) hemicellulose structure.....	29
Figure 4.2	(A) Photographic image and (B-D) OM images of raw PALF, alkali-treated PALF, and bleached PALF. ....	30
Figure 4.3	The cleavage reaction of the $\beta$ -O-4 aryl ether bond in lignin during alkali treatment. ....	31
Figure 4.4	The reaction of $H_2O_2$ activation in alkali condition.....	32
Figure 4.5	The reaction of the phenolate groups in lignin was oxidized into carboxylate in bleaching treatment. ....	32
Figure 4.6	FT-IR spectra of raw PALF, alkali-treated PALF, and bleached PALF.	33
Figure 4.7	FT-IR spectra of bleached PALF, filter paper, Kim-Tech, Avicel PH101, and bacterial cellulose (BC).....	36
Figure 4.8	(A) TGA and (B) DTG thermograms of raw PALF (black), alkali-treated PALF (red), and bleached PALF (blue).....	39
Figure 4.9	Drawing illustration of cellulose structure in bleached PALF consists of amorphous and crystalline regions.....	40
Figure 4.10	OM images of (A) bleached PALF, (B) -20PALF25%, (C) 30PALF25%, (D) 50PALF25%, and (E) Avicel PH101 and corresponding size distribution. ....	42
Figure 4.11	The reaction of hydrolysis in sulfuric acid treatment. ....	43
Figure 4.12	Drawing illustration of partial hydrolysis occurred, forming microcrystalline cellulose (MCC).....	44
Figure 4.13	FT-IR spectra of bleached PALF, -20PALF25%, 30PALF25%, 50PALF25%, and Avicel PH101 at $3900-600\text{ cm}^{-1}$ region. ....	46
Figure 4.14	(A) TGA and (B) DTG thermograms of bleached PALF (black), -20PALF25% (red), 30PALF25% (blue), and 50PALF25% (green).....	47

Figure 4.15	OM images of (A) bleached PALF, (B) -20PALF50%, (C) 30PALF50%, (D) 50PALF50%, cross-polarizer images, and corresponding size distribution of lengths and widths.....	49
Figure 4.16	Transformation of (A) bleached PALF into (B) cellulose solution, then regenerate into (C) RAC after washed with DI water.....	50
Figure 4.17	Chemical reaction of the dissolution process in cellulose. ....	51
Figure 4.18	Drawing illustration of RAC transformation in 50% H <sub>2</sub> SO <sub>4</sub> at -20 °C...	52
Figure 4.19	Partial hydrolysis occurred, forming microcrystalline cellulose (MCC).....	52
Figure 4.20	Photographic image of -20PALF50%, 30PALF50%, and 50PALF50%.....	53
Figure 4.21	Drawing illustration of hydrolysis at 50 °C of 50% (v/v) H <sub>2</sub> SO <sub>4</sub> , forming nanocrystalline cellulose (NCC).....	54
Figure 4.22	FT-IR spectra of bleached PALF, -20PALF50%, 30PALF50%, and 50PALF50% in the (A) 3900-2700 cm <sup>-1</sup> and (B) 1800-600 cm <sup>-1</sup> regions. ....	55
Figure 4.23	X-ray diffraction (XRD) patterns recorded from bleached PALF (black), -20PALF50% (red), 30PALF50% (blue), and 50PALF50% (green) samples.....	58
Figure 4.24	(A) TGA and (B) DTG thermograms of bleached PALF (black), -20PALF50% (red), 30PALF50% (blue), and 50PALF50% (green). ....	60

## LIST OF ABBREVIATIONS

PALF	: pineapple leaf fiber
H <sub>2</sub> SO <sub>4</sub>	: sulfuric acid
H <sub>3</sub> PO <sub>4</sub>	: phosphoric acid
NaOH	: sodium hydroxide
H <sub>2</sub> O <sub>2</sub>	: hydrogen peroxide
CNT	: carbon nanotube
MCC	: microcrystalline cellulose
NCC	: nanocrystalline cellulose
NFC	: nanofibril cellulose
RAC	: regenerated amorphous cellulose
OM	: optical microscope
XRD	: x-ray diffractometer
FT-IR	: Fourier-transform infrared spectrometer
TGA	: thermogravimetric analysis
DTG	: derivate Thermogravimetric
TEM	: transmission electron microscope
SEM	: scanning electron microscope
CI	: crystallinity index
H <sub>2</sub> O	: water
L	: length
D	: diameter or width
min	: minute
h	: hour
g	: gram
mg	: milligram
mL	: milliliter
cm	: centimeter
µm	: micrometer
%	: percent
α	: alpha

$\beta$	: beta
$\delta$	: bending
$\gamma$	: stretching
$\theta$	: theta
$^{\circ}\text{C}$	: degree Celsius
DI water	: de-ionized water
T	: temperature
RT	: room temperature
BC	: bacterial cellulose
3D	: three-dimensional
v/v	: volume per volume
w/v	: weight per volume
I	: intensity
$\text{cm}^{-1}$	: wavenumber
et al.	: et al ii, in Latin meaning “and others”



# CHAPTER I

## INTRODUCTION

### 1.1 Research background

Nowadays, sustainable concern has raised great attention. This concern motivates people to maximize the utility of renewable resources and minimize the production of industrial residues. Cellulose is the most abundant natural polymer on earth, with 1.5 trillion tons produced each year<sup>1</sup>. Cellulose can be derived from agricultural products and residues. Cellulose consists of linear homopolysaccharide composed of unbranched glucose units linked by  $\beta$ -1,4-glycosidic linkages. Cellulose has strong inter and intramolecular H-bonding from glucose unit that carries three hydroxyl groups, causing it remains insoluble in most solvents<sup>2</sup>. Cellulose possesses significant advantages, such as high molecular order, biodegradability, biocompatibility, non-toxic, and good thermal stability, making cellulose an attractive “green” material<sup>3</sup>. Cellulose has been widely used in the textile industry, sensing, food, composite material, and biomedical applications.

Pineapple is one of the most favorite tropical fruit that is widely cultivated. Due to its popularity for food and beverage consumption, pineapple contributes to approximately 1 million tons of agricultural residue annually in Thailand<sup>4</sup>. Pineapple leaves are the major residue of pineapple plants (1 million tons of leaves with 1.79 million tons of pineapple production)<sup>5</sup>. Pineapple leaf fiber (PALF) has high cellulose content (74%) that can be a great resource for cellulosic products<sup>6</sup>.

Despite the high potential of PALF usage, there is still a huge amount of pineapple leaf residue that makes the farmers prefer to burn the pineapple leaf residue to clean their field. This burning creates more problems in sustainable concern due to generating air pollution<sup>7</sup>. Comprehensive work must be done to reduce the residue and increase more value on the PALF. By turning PALF into cellulosic products, it will advance cellulose applications and increase the value of PALF.

Cellulosic products can be categorized as microcrystalline (MCC), nanofibril (NFC), nanocrystal (NCC), and regenerated amorphous cellulose (RAC)<sup>8, 9</sup>. NCC is very popular in the cellulose research field, which most of the researchers have

worked for this. NCC has advantages such as high tensile strength, high modulus, high hydrophilicity, high dispersion, large surface area, unique optical properties<sup>10, 11</sup>. But NCC has a low yield (~ 24%) due to the process of how NCC was formed<sup>12</sup>. Cellulose has the amorphous and crystalline region on its structure. The amorphous region will be destroyed by the hydrolysis agent, and the crystalline region will be preserved in the process of making NCC. However, the hydrolysis agent has poor selectivity for the amorphous region, as some of the crystalline region has also been degraded. As a consequence, the NCC production has a low yield<sup>13</sup>.

In this research, we focus on preparing RAC from PALF via sulfuric acid treatment at low-temperature (-20 °C) and following the changes in the process of producing RAC by spectroscopic and morphological characterizations. Transforming PALF into RAC will give a higher yield (yield ~97.4%)<sup>14</sup> than to NCC due to the sulfuric acid interaction mechanism with cellulose. The RAC can be used as a potential alternative for the same application with NCC, such as a reinforcing agent, composite material, and water in oil emulsions stabilizer<sup>15, 16</sup>. At low-temperature (-20 °C), sulfuric acid will majorly break down the inter and intramolecular H-bonding among cellulose molecules, dissolving the amorphous and crystalline regions together, but only minor cleaving the cellulose chain under the acid hydrolysis reaction<sup>17</sup>. At high temperature (i.e., >50 °C), which obtaining NCC, sulfuric acid will destroy the amorphous region of the cellulose fiber by hydrolysis, while the crystalline region remains unaffected<sup>18</sup>.

## 1.2 The objectives

1. To develop processes for large scale production of regenerated amorphous cellulose.
2. To develop economical purification processes of regenerated amorphous cellulose.
3. To perform spectroscopic and structural characterization of the regenerated amorphous cellulose.

## 1.3 The scopes of research

1. Purification of the PALF using alkali and bleaching treatment.
2. Characterization of PALF using an optical microscope (OM) and Fourier transform infrared (FT-IR) spectroscopy.
3. Hydrolysis of the PALF into nanocrystalline cellulose via high temperature sulfuric acid treatment.
4. Dissolution of the PALF in cold  $H_2SO_4$ .
5. Regeneration of the cellulose solution by adding the water as an anti-solvent.
6. Purification of the regenerated amorphous cellulose and nanocrystalline cellulose.
7. Characterization of the morphology and chemical structural changes in the regenerated amorphous cellulose and nanocrystalline cellulose with XRD, FT-IR, and TGA characterization.

## CHAPTER II

### THEORETICAL BACKGROUND

#### 2.1 Pineapple leaf fiber (PALF)

Jirapornvaree et al. (2017) reported that pineapple production in Thailand has reached about 1.7 million tons annually, making Thailand the fourth-largest producer and exporter of pineapple in the world. From this huge production, Thailand could generate pineapple leaf wastes about 1 million tons approximately<sup>4,5</sup>.

Pineapple leaf fiber (PALF) is an essential natural fiber that displays high stiffness and strength with a ribbon-like structure that consist of a vascular bundle system present in bunches of fibrous cells obtained after removing the epidermal tissue mechanically (Figure 2.1). PALF is of high quality, and its structure is without mesh and can be turned into nanofibers thinner than fibers from bacterial cellulose (BC) and tunicates<sup>19</sup>.



Figure 2.1 Production of pineapple leaf fiber, sequential (A) pineapple plant, (B) extraction of fiber from pineapple leaves, and (C) pineapple leaf fiber. Copyright 2015 Hindawi Publishing Corporation<sup>20</sup>.

##### 2.1.1 Cellulose content in PALF compared with other agricultural wastes

The cellulose content of PALF was the highest compared to other agricultural wastes. The high cellulose content in PALF can be an advantage in producing cellulosic products from PALF. The list of cellulose content in agricultural wastes was written in Table 2.1 below.

Table 2.1 Cellulose content in agricultural wastes.

Material	Cellulose (%)	Ref.
PALF	74	6
Rice husk	35	21
Wheat straw	30	22
Soy hulls	48	23
Kenaf bast fibers	44	24
Bagasse pith	40	25
Corn cobs	35	26

The calculations are based on a dry basis

## 2.1.2 Purification in PALF

### 2.1.2.1 Major impurities in PALF

PALF not only consists of cellulose but also some impurities attached to the fiber. Maniruzzaman et al. (2016) reported that on a dry basis, PALF contains cellulose about 74.24% with hemicellulose 12.6% and lignin 7.14% as its main impurities<sup>6</sup>.

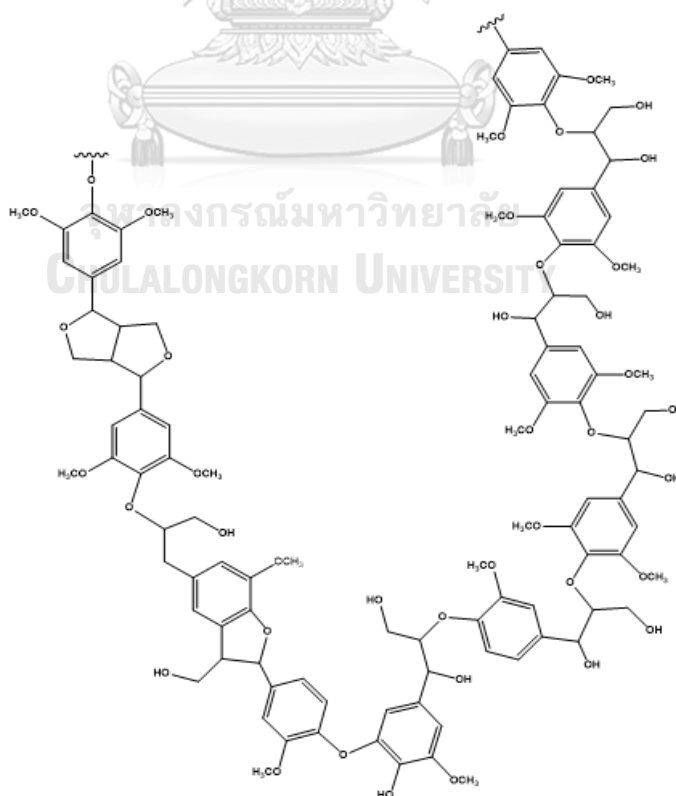


Figure 2.2 Chemical structure of lignin<sup>27</sup>.

Lignin exists in an abundant aromatic (phenolic) polymer in nature<sup>28</sup>. Its main function is cementing the cellulose fibers in plants. Biological functions of lignin in vascular plants are to promote rigidity, also to protect the structural polysaccharides cellulose and hemicellulose from enzymatic hydrolysis. Lignin is a heterogeneous, crosslinked with a highly polydisperse phenolic copolymer of three different monolignols: p-coumaryl alcohol, coniferyl alcohol, and sinapyl alcohol<sup>29</sup>. The chemical structure of lignin was shown in Figure 2.2.

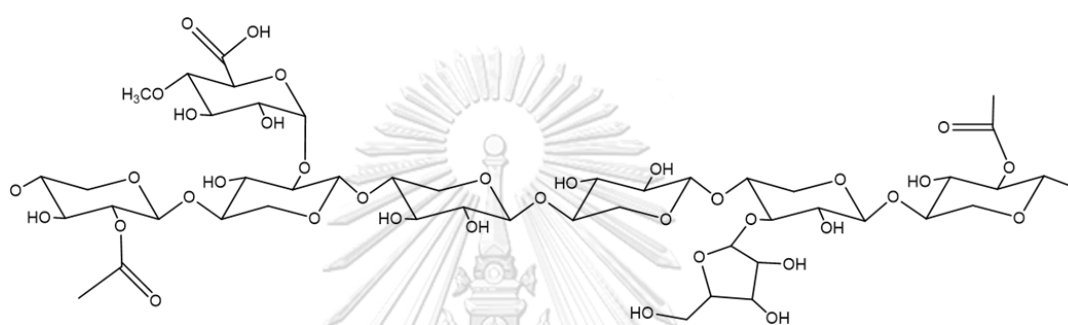


Figure 2.3 Chemical structure of hemicellulose<sup>30</sup>.

Hemicellulose with a random ordered structure is located within the cellulose and between the cellulose and lignin<sup>31</sup>. Hemicellulose structure consists of pentoses such as xylose and arabinose, hexoses such as glucose, mannose, galactose, and sugar-acid<sup>32</sup>. The chemical structure of hemicellulose was shown in Figure 2.3.

#### 2.1.2.2 Advantages and disadvantages of purification treatment

Purification treatment is needed in order to obtain pure cellulose by removing lignin and hemicellulose from the PALF. Purification treatment with high effectivity, simplicity, and low cost is favorable. Based on these reasons, the advantages and disadvantages of the treatment have been made in Table 2.2.

Table 2.2 Advantages and disadvantages in purification treatment.

Method	Advantages	Disadvantages	Ref.
Dilute Acid	<ul style="list-style-type: none"> <li>• Operation time is less</li> <li>• High effectivity</li> <li>• Can be for large scale production</li> </ul>	<ul style="list-style-type: none"> <li>• Acid recovery</li> <li>• Generate the high amount of inhibitory products</li> </ul>	33
Organosolvosis	High effectivity	<ul style="list-style-type: none"> <li>• Solvent recovery is expensive</li> </ul>	34
Milling	<ul style="list-style-type: none"> <li>• Operation time is less</li> <li>• No require chemical</li> <li>• Can be for large scale production</li> </ul>	<ul style="list-style-type: none"> <li>• Effectivity is low</li> <li>• Expensive instrument</li> </ul>	35
Peroxide-Acetic Acid	High effectivity	Need assistance for more strong acid	36
Steam explosion	No inhibitory compounds	Maintaining high pressure itself is a challenge	37
Alkali treatment	<ul style="list-style-type: none"> <li>• High Effectivity</li> <li>• Can be done at room temperature</li> <li>• Low cost</li> <li>• Simple purification</li> <li>• Can be for large scale production</li> </ul>	In high concentration of NaOH, defect on mechanical properties of fibers could be occurred	38
H <sub>2</sub> O <sub>2</sub> bleaching	<ul style="list-style-type: none"> <li>• Environmental friendly</li> <li>• Strong oxidizing agent</li> <li>• Low cost</li> <li>• Simple purification</li> </ul>	Fast degraded of H <sub>2</sub> O <sub>2</sub>	39

This work required a low cost, high effectivity, and environmental friendly in the process. Alkali treatment assisted with H<sub>2</sub>O<sub>2</sub> bleaching is the most required treatment for this work.

## 2.2 Cellulose

### 2.2.1 Cellulose structure

Cellulose has a linear chain of ringed glucose molecules. The repeat unit is comprised of two anhydroglucose rings ( $(C_6H_{10}O_5)_n$ ;  $n = 10\,000$  to  $15\,000$ , where  $n$  is dependent on the cellulose source material) connected together through covalent bonding of oxygen to C1 of one glucose ring and C4 of the adjoining ring (1→4 linkages), named as  $\beta$ -1,4-glycosidic linkages. The intrachain H-bonding bonded between OH groups and oxygens of the adjacent ring molecules stabilizes linkages, making a linear configuration of the cellulose chain<sup>40</sup>. Cellulose structure and the inter and intramolecular H-bonding was displayed in Figure 2.4.

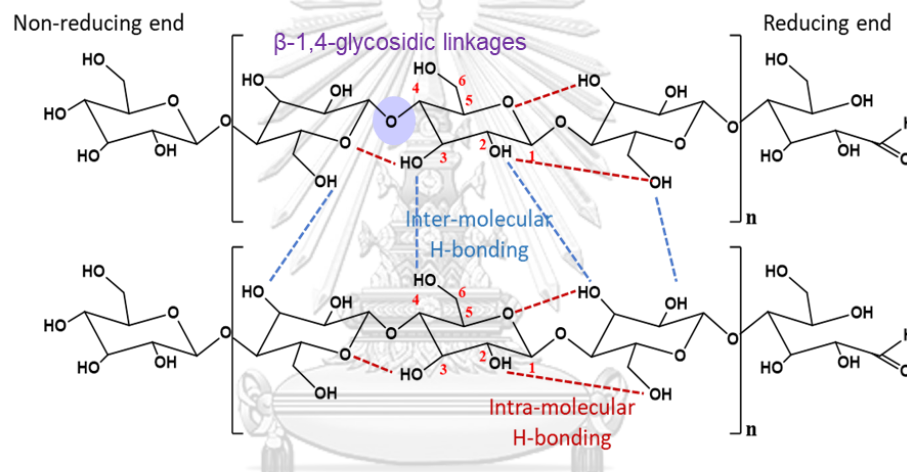


Figure 2.4 Structure of cellulose and its inter and intramolecular H-bonding<sup>41</sup>.

Van der Waals and intermolecular H-bonding between OH groups and oxygens of adjacent molecules provide parallel stacking of multiple cellulose chains obtaining elementary fibrils that further bundle into larger microfibrils (5–50 nm in diameter and several microns in length). The intra and intermolecular H-bonding network builds a strong and stable cellulose, providing the cellulose fibrils with high axial stiffness. These cellulose fibrils are the main reinforcement phase for trees, plants, some marine creatures (tunicates), algae, and bacteria, making there are regions where the cellulose chains are arranged in highly ordered (crystalline) and disordered (amorphous) regions (Figure 2.5)<sup>42</sup>.

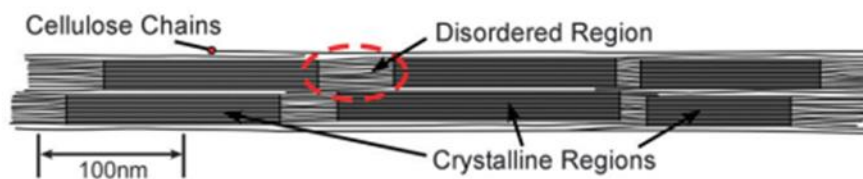


Figure 2.5 Crystalline and amorphous (disordered) regions in cellulose. Copyright 2011 The Royal Society of Chemistry<sup>40</sup>.

## 2.2.2 Cellulosic products

For advanced applications, cellulose generally develops into cellulosic products that typically differ based on its particle size.

### 2.2.2.1 Microcrystalline cellulose (MCC)

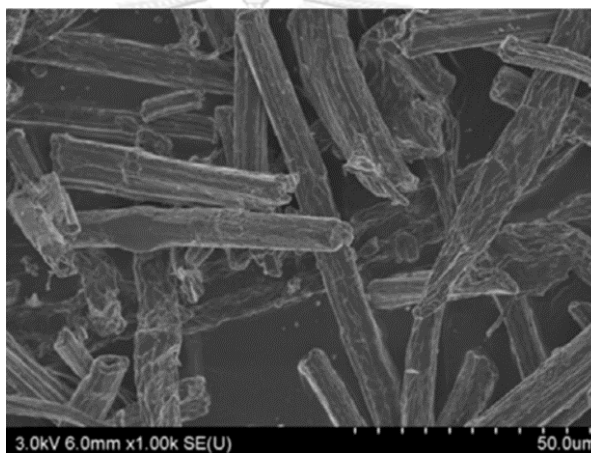


Figure 2.6 Morphology of MCC in SEM images. Copyright 2014 Elsevier Ltd<sup>43</sup>.

MCC is prepared by partial acid hydrolysis of native cellulose. MCC is generally used in pharmaceutical (tablet binder), food (rheology control agent), paper, and composites manufacturings<sup>44</sup>. MCC has micro-sized rod-like particles (Figure 2.6), with length and width about 10-200  $\mu\text{m}$  and 30 nm-20  $\mu\text{m}$ , respectively. MCC has a high cellulose content and a higher crystallinity and comprises aggregate bundles of multi-sized cellulose microfibrils strongly H-bonding to each other<sup>40, 45</sup>.

### 2.2.2.2 Nanocrystalline cellulose (NCC)

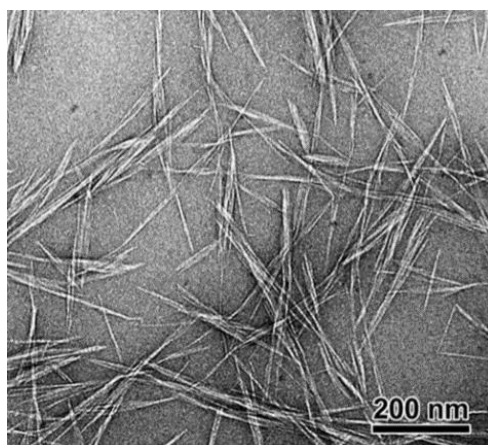


Figure 2.7 Morphology of NCC shown in the TEM image. Copyright 2016 The Royal Society of Chemistry<sup>46</sup>.

Nanocrystalline cellulose (NCC) is formed when cellulose consist of amorphous and crystalline regions are subjected to a proper combination of mechanical, chemical, and enzyme treatments, the highly ordered regions of the cellulose microfibrils can be extracted, resulting in the formation of NCC. NCC was stiff rod-like shape material (Figure 2.7) composing of cellulose chain portions in a nearly perfect crystalline structure. Habibi et al. (2011) mentioned that NCC has a length and width of about 50 nm-3  $\mu\text{m}$  and 3-70 nm, respectively<sup>42</sup>. Compared to bulk cellulose, which has more significant amorphous composition, NCC exhibit high specific strength, modulus, high surface area, and unique liquid crystals properties<sup>18, 47, 48</sup>. Due to its excellent properties, NCC is popular in the research field for many various applications.

Jiang et al. (2019) made a composite film using carbon nanotube and NCC. Conductive CNT + NCC hybrid films (5–20  $\mu\text{m}$  thick) were cast on glass microscope slides with and without shear by blade coating<sup>49</sup>.

Kalashnikova et al. (2012) applied NCC as an oil/water stabilizer. An emulsion able to be dispersed in water and resistant to centrifugation at 4000g was obtained from NCC<sup>50</sup>.

Although NCC can apply in many applications, it has a disadvantage corresponding to its low yield because of removing the amorphous region and some defects in the crystalline region due to the obtaining process<sup>51</sup>.

### 2.2.2.3 Nanofibril cellulose (NFC)

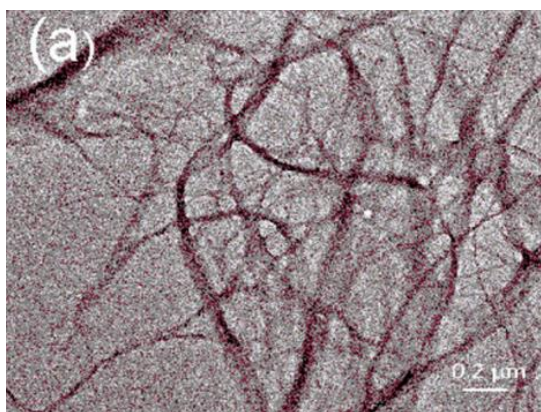


Figure 2.8 Morphology of NFC displayed in the TEM image. Copyright 2018 WILEY-VCH Verlag GmbH & Co. KGaA<sup>52</sup>.

Nanofibril cellulose (NFC) was obtained using mild acid hydrolysis or ball milling to retain their fibrous structure. Cellulose nanofiber consists of crystalline and amorphous regions<sup>52</sup>. NFC's width ranged from 10 to 90 nm, regardless of the cellulose fibers used, whereas the length was estimated to be on a micrometer scale<sup>24</sup>. The morphology of NFC was displayed in Figure 2.8.

Uddin et al. (2018) applied CNF as microfluidic channels for glucose detection due to its nanoscale dimensions and the strong ability to form entangled porous networks<sup>53</sup>.

#### 2.2.2.4 Regenerated amorphous cellulose (RAC)

Regenerated amorphous cellulose (RAC) is the most different cellulosic product. Compared with the extensive research on the crystalline form of cellulose, less research has been devoted to the amorphous form of cellulose. It does not have a fibrous morphology but a unique gel-like shape morphology (Figure 2.9). It was formed by breaking inter and intramolecular H-bonding<sup>17</sup>. In this state, the crystalline and amorphous regions of native cellulose were dissolved together into cellulose solution without any removal. Then, after adding water into the solution, RAC made a new arrangement in a random manner, resulting in a gel-like shape<sup>14, 16, 17</sup>.

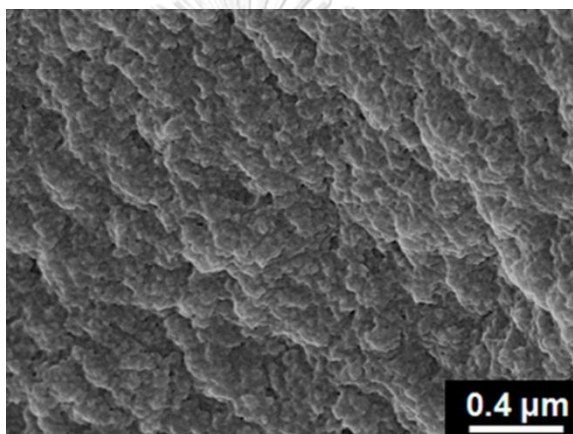


Figure 2.9 Morphology of RAC showed in the SEM image. Copyright 2019 American Chemical Society<sup>54</sup>.

Jia et al. (2013) reported that RAC could be a potential alternative for NCC in some applications that do not need crystalline properties. The yield was also so high, almost 100%, because the crystalline and amorphous were mixed in the process, without any removal<sup>16</sup>.

## 2.3 Methods to obtain RAC

### 2.3.1 N-methylmorpholine-N-oxide (NMMO)

N-methylmorpholine-N-oxide (NMMO) has been used as an organic solvent for the preparation of cellulose solutions. It is applied as a non-derivatizing solvent in the cellulose dissolution procedure. The cellulose is supposed to undergo an entirely physical process during dissolution due to the H-bonding and ionic interactions between NMMO and cellulose. NMMO is a green solvent for cellulose dissolution. Still, the drawback of NMMO is the requirement of activation before dissolution, instability, the side reaction of the solvent itself without an antioxidant, difficulty for recycling, and its high cost as well<sup>55</sup>. The summary of work using NMMO was listed in Table 2.3.

Table 2.3 Summary of work using NMMO.

Cellulose Source	Solvent	T (°C)	Note	Reference
Bleached linter pulp	NMMO	210 Watt	<ul style="list-style-type: none"> <li>The requirement of activation before the dissolution</li> <li>High cost</li> </ul>	Dogan, <i>Carbohydr. Polym.</i> , 2009

### 2.3.2 Inorganic salts

Hattori et al. (2016) proposed mixtures of small amines and certain inorganic salts can dissolve cellulose without degrading it. But the method is not convenient because it took about 3 days to dissolve the cellulose completely and also needs to be stirred every 6 hours<sup>56</sup>. The summary of work using inorganic salts was listed in Table 2.4.

Table 2.4 Summary of work using inorganic salts.

Cellulose Source	Solvent	T (°C)	Note	Reference
MCC	NaSCN	RT	The dissolution was completed in 3 days	Hattori, <i>ACS Sustainable Chem. Eng.</i> , 2016

### 2.3.3 Ionic liquids (IL)

Ionic liquids (IL) are salts that exist as a liquid at relatively low temperatures (less than 100 °C), with many attractive properties such as nonvolatile, chemical and thermal stability, non-flammability, and immeasurably low vapor pressure<sup>57</sup>. Works of Tan et al. (2019) and Iguchi et al. (2013) have done using IL at high temperature (90-120°C), which means IL consumes more energy to be done<sup>58, 59</sup>. Cellulose dissolution also took a long time to dissolve, around 3-5 hours completely. The summary of work using IL was listed in Table 2.5.

Table 2.5 Summary of works using IL.

Cellulose Source	Solvent	T (°C)	Note	Reference
MCC	[Emim][OAc]	90	Regenerated using anti-solvent water would lead to the small forming amount of cellulose II, while ethanol did not show the peak corresponding to cellulose II in XRD patterns.	Tan, <i>Int. J. Biol. Macromol.</i> , 2019
MCC	[bmIm][Cl]	120	RAC in this work still has high crystallinity (50-70%)	Iguchi, <i>Carbohydr. Polym.</i> , 2013

### 2.3.4 NaOH/Urea

Cai et al. (2008) mentioned that NaOH “hydrates” could be more easily attracted to cellulose chains through the formation of new H-bonding networks, relatively stable at low temperatures. Whereas, the urea hydrates as shell surrounded the NaOH-cellulose to form an inclusion complex (IC) with sheath-like structure, leading to the dissolution of cellulose<sup>60</sup>. But this method is less useful for high molecular weight samples like wood, so it needs to be partially hydrolyzed for full dissolution in NaOH/Urea aqueous<sup>17</sup>. The summary of work using NaOH/Urea was listed in Table 2.6.

Table 2.6 Summary of works using NaOH/Urea.

Cellulose Source	Solvent	T (°C)	Note	Reference
Cotton linter	7% (w/v) NaOH 12% (w/v) urea	-12	Fast dynamic self-assembly process among small solvent molecules and cellulose macromolecules	Cai, J. <i>Macromolecules</i> , 2015

### 2.3.5 LiCl/N,N-dimethylacetamide (LiCl/DMAc)

LiCl/N; N-dimethylacetamide (LiCl/DMAc) is a nonaqueous solvent system that has been widely applied to dissolve different cellulose types without necessary degradation for cellulose modification under homogenous reaction conditions to prepare a wide range of derivatives. It is noted that LiCl/DMAc can dissolve cellulose with high molecular weight (>1000,000) at ambient temperature without noticeable degradation.<sup>3</sup> The work of Dupont et al. (2003) reported that the product is stable for several months, but the water has to be excluded from the system because LiCl and DMAc are very hygroscopic. Considering the solvent preparation is complicated, this method is not the most convenient one to choose<sup>61</sup>. The summary of work using LiCl/DMAc was listed in Table 2.7.

Table 2.7 Summary of work using LiCl/DMAc.

Cellulose Source	Solvent	T (°C)	Note	Reference
Filter paper	LiCl/DMAc	50-100	<ul style="list-style-type: none"> <li>Product is stable until several months</li> <li>Water has to be excluded from the system (LiCl and DMAc are very hygroscopic)</li> <li>Solvent preparation is complicated</li> </ul>	Dupont, <i>Polymer</i> , 2003

### 2.3.6 Acid treatment

Jia et al. (2013) reported that acid treatment provides a simple process to dissolve cellulose. Direct dissolution of cellulose in 85% (w/v) H<sub>3</sub>PO<sub>4</sub> was difficult

because the dry cellulose powder dissolved rapidly and produced a viscous layer that made the solvent penetrated very slowly. Prewetting of the cellulose powder was needed to achieve a quick dissolution. It took 5 hours to dissolve the cellulose completely<sup>16</sup>. Huang et al. (2016) reported that H<sub>2</sub>SO<sub>4</sub> took 5 min to dissolve a high molecular weight sample without any prewetting<sup>17</sup>. This result suggested that H<sub>2</sub>SO<sub>4</sub> is more powerful, quick, and direct to dissolve the cellulose. In this work, H<sub>2</sub>SO<sub>4</sub> treatment was chosen to obtain RAC from PALF. The summary of work using acid treatment was listed in Table 2.8.

Table 2.8 Summary of work using the acid treatment.

Cellulose Source	Solvent	T (°C)	Note	Reference
MCC	85% (w/v) H <sub>3</sub> PO <sub>4</sub>	-	Yield of RAC: 85.6 ± 1.1%	Jia, <i>J. Agric. Food Chem.</i> , 2013
Bleached kraft pulp	64 (v/v) % H <sub>2</sub> SO <sub>4</sub>	-20	Simple process, powerful, quick, and direct solvent for high molecular weight cellulose	Huang, <i>Cellulose</i> , 2016

#### 2.4 Applications of RAC

Qi et al. (2013) fabricated multifunctional carbon nanotube (CNT)–cellulose films by dissolving cellulose and dispersing CNTs homogeneously in aqueous alkaline–urea solution. The obtained composite films with 2-10 wt% CNTs have both characteristics of normal flexible paper and conducting CNT, which show a volume resistivity controlled over a wide range of 1.35–540 Ohm cm. The composite films accomplished multifunctional sensing ability to monitor stress-strain, temperature, and humidity. The composite films with CNTs were enhanced of both their thermal and mechanical stabilities. The morphology and microstructure of CNT-cellulose composite films were displayed in Figure 2.10.

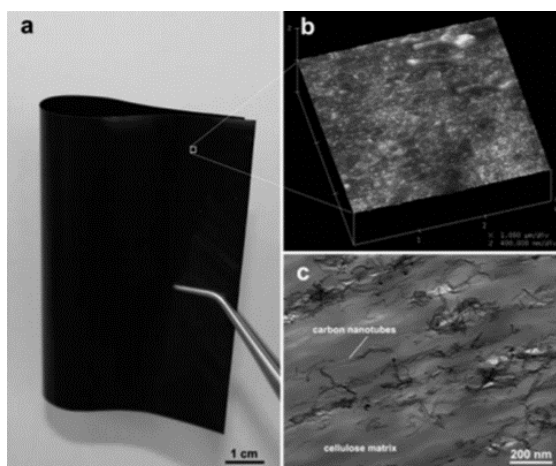


Figure 2.10 Morphology and microstructure of the CNT-cellulose composite films regenerated from NaOH-Urea aqueous solution: (a) photograph, (b) AFM image, and (c) TEM image. Copyright 2013 The Royal Society of Chemistry<sup>62</sup>.

Zhang et al. (2015) reported the amorphous cellulose film (ACF) that was prepared from cellulose solution in LiCl (8 wt%)/DMAc by regeneration with acetone had a solid, smooth surface, and high transparency. The image of the ACF was displayed in Figure 2.11.



Figure 2.11 The image of a transparent film of CF11 6%. Copyright 2015 The Royal Society of Chemistry<sup>63</sup>.

## CHAPTER III

### EXPERIMENTAL SECTION

#### 3.1 Chemical reagents

1. Pineapple leaf fiber, PALF (local farmers, Thailand)
2. Sodium hydroxide, NaOH (Merck & Co., Germany)
3. Sulfuric acid, H<sub>2</sub>SO<sub>4</sub> (95-97% (v/v)) (Merck & Co., Germany)
4. Hydrogen peroxide, H<sub>2</sub>O<sub>2</sub> (50% (v/v)) (Solvay Peroxythai Ltd., Thailand)
5. Kim-Tech wipes (Kimberly-Clark Ltd., Thailand)
6. Filter paper (Johnson test paper Ltd., Thailand)
7. Avicel PH-101 (Sigma Aldrich Ltd., Thailand)
8. De-ionized (DI) water

#### 3.2 Instruments

1. Centrifuge (Hettich EBA 200, Hettich GmbH & Co., Germany)
2. Refrigerator (Hitachi R-H200PA-1, Hitachi Asia Co., Ltd., Thailand)
3. Digital thermometer (TP300)
4. Optical microscope, OM (Axio Scope. A1 with a CCD camera, AxioCam HRc, Carl Zeiss Co., Ltd., Germany)
5. Fourier-transform infrared spectrometer, FT-IR (iD7 ATR Nicolet, Thermo Fisher Scientific Inc., US)
6. Hotplate stirrer (MR Hei-standard, Heidolph GmbH & CO.KG, Germany)
7. Thermogravimetric analyzer, TGA (Pyris 1 TGA, Perkin Elmer Inc., UK)
8. X-ray diffractometer, XRD (RINT2000, Rigaku Corp., Japan)

### 3.3 Purification of raw PALF

#### 3.3.1 PALF pretreatment

The raw PALF was cleaned using tap water to remove the water-soluble dirt. After it was clean, the raw PALF was cut into short fibers with lengths ~10 cm. The cutting was done to process for the next treatment effectively. The cut PALF was kept in the plastic bag for further usages.

#### 3.3.2 Alkali treatment

The cut PALF (50 g) was boiled in NaOH (4% (w/v), 500 mL) for 2 h under mechanical stirring. The alkali treatment started to occur when the solution became yellow. The alkali-treated PALF was washed with DI water until a neutral pH was obtained.

#### 3.3.3 Bleaching treatment

The mixture solution of H<sub>2</sub>O<sub>2</sub> (50% (v/v), 25 mL) and NaOH (0.1% (w/v), 500 mL) was prepared. The alkali-treated PALF was immersed and boiled in the mixture solution for 1 h under mechanical stirring. The bleached PALF was washed with DI water to reach a neutral pH. Then, it was kept in the refrigerator for further usages.

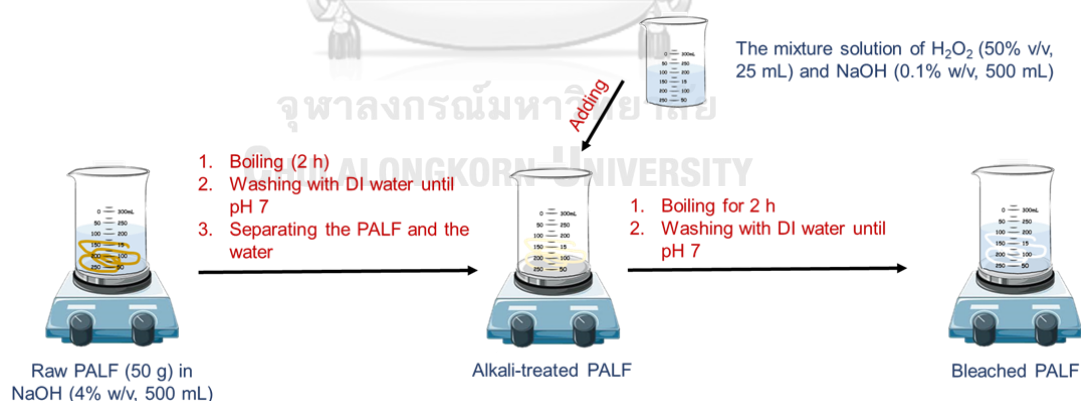
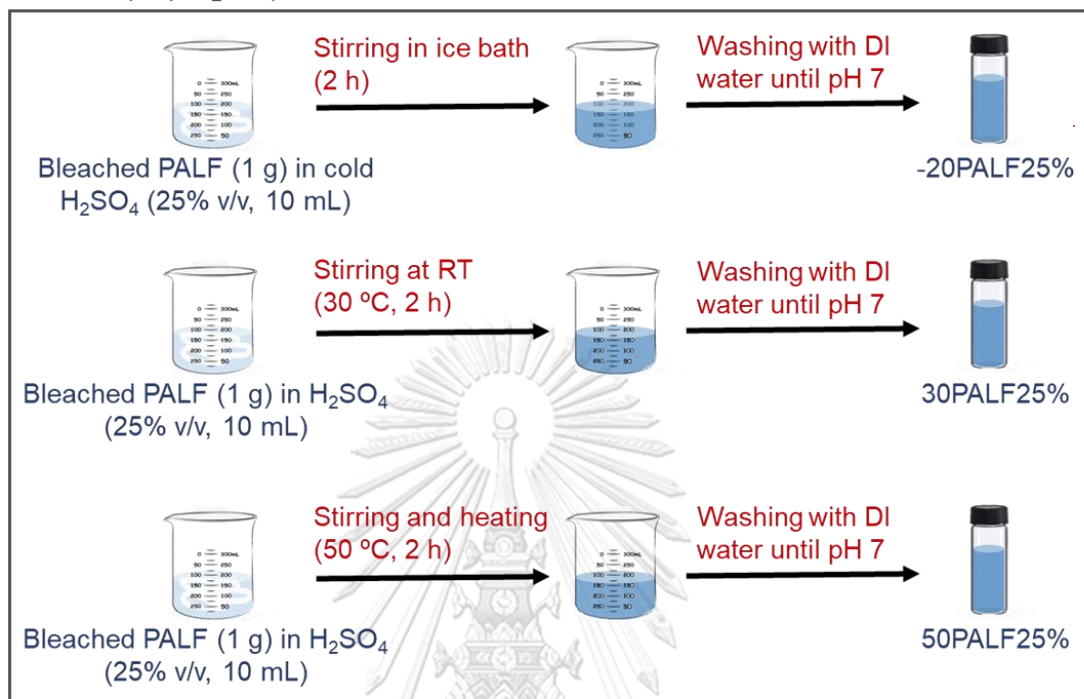


Figure 3.1 Purification of PALF using alkali and bleaching treatments.

### 3.4 Preparation of cellulosic products from bleached PALF via sulfuric acid treatment

A: 25% (v/v)  $\text{H}_2\text{SO}_4$



B: 50% (v/v)  $\text{H}_2\text{SO}_4$

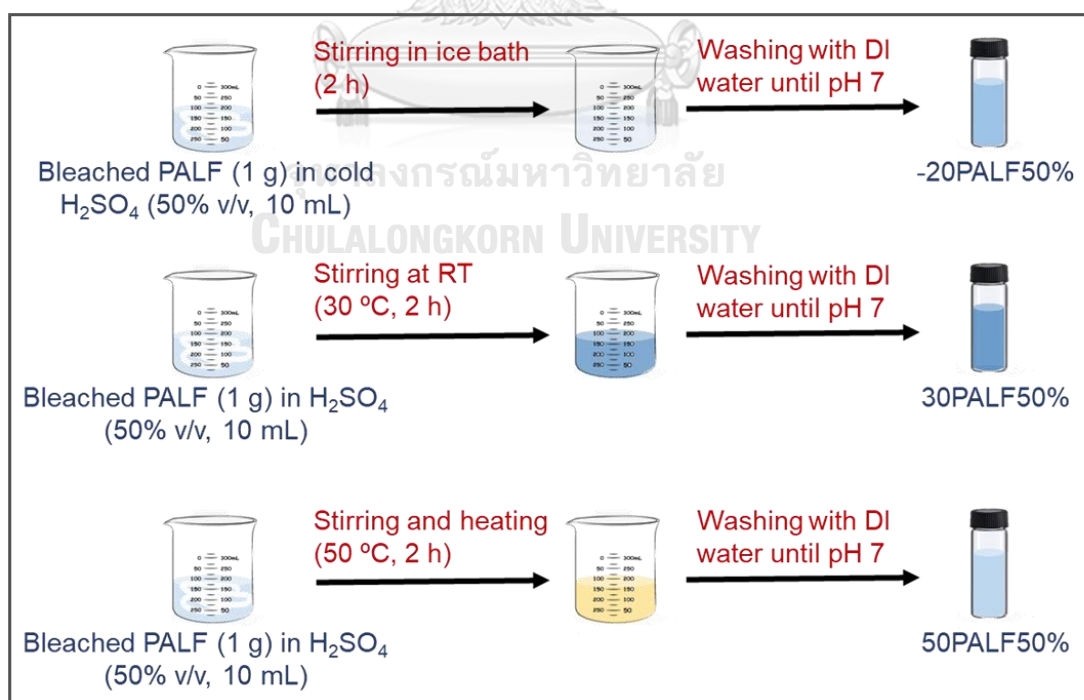


Figure 3.2 Sulfuric acid treatment of PALF in (A) 25% and (B) 50% (v/v)  $\text{H}_2\text{SO}_4$ .

The bleached PALF (1 g) was treated with H<sub>2</sub>SO<sub>4</sub> (10 mL) with continuous stirring under different conditions as follows: 25% and 50% (v/v) H<sub>2</sub>SO<sub>4</sub> solution. Each concentration was treated at -20 °C, 30 °C, and 50 °C for 2 h. As noted at -20 °C, we pre cold the H<sub>2</sub>SO<sub>4</sub> (placed the H<sub>2</sub>SO<sub>4</sub> in the refrigerator) to prevent the increasing temperature at the system. The reactions were terminated by adding an excess (10-fold) cold DI water. The acidic solution was removed by successive centrifugation at 6000 rpm for 15 min. The precipitate was washed with DI water and centrifuged it several times. Then, the precipitate was collected after reaching a neutral pH. The cellulosic products were labeled “Temperature-PALF-Sulfuric acid concentration”. For example, “-20PALF25%” means the PALF in 25% v/v H<sub>2</sub>SO<sub>4</sub> and -20° C condition. The process was illustrated in Figure 3.2.

### **3.5 Characterizations**

#### **3.5.1 Optical microscopy (OM)**

Morphologies of the raw PALF, alkali-treated PALF, bleached-PALF, and all cellulosic products were characterized using an optical microscope (OM) (Axio Scope. A1 with a CCD camera, Carl Zeiss) with magnifications of 50X, 100X, 200X, 500X, 1000X by putting the sample on the glass slide.

#### **3.5.2 Fourier-transform infrared (FT-IR) spectroscopy**

The raw PALF, alkali-treated PALF, bleached PALF were dried using an air-circulated oven at 100 °C. Cellulosic products were dried by a vacuum desiccator on a glass slide to form the thin film. Kim-Tech wiper and filter paper were directly put on the FT-IR spectrometer, respectively. FT-IR spectra of the raw PALF, alkali-treated PALF, bleached PALF, Kim-Tech, filter paper, and all cellulosic products were collected using a Fourier-transform infrared spectrometer (FT-IR) (iD7 ATR Nicolet, Thermo Scientific). The FT-IR spectra were recorded over the range of 4000–400 cm<sup>-1</sup> with 16 co-addition scans.

### 3.5.3 Birefringence analysis

Each cellulosic product from sulfuric acid treatment was prepared in the same concentration (0.1 g/mL) and placed in the 3 mL glass vial. These bottles were placed in a cross-polarized attachment and photographed by a smartphone camera.

### 3.5.4 Thermal gravimetric analysis (TGA)

The thermal properties of PALF were determined by using a thermogravimetric analysis (TGA) instrument (Pyris 1 TGA, Perkin Elmer). The process was carried out under nitrogen gas flow at the rate of 50 cm<sup>3</sup>/min. The samples were prepared by placing a various amount of raw PALF, alkali-treated PALF, bleached PALF, and cellulosic products with 1 mg of sample on a crucible ceramic pan. The samples were heated from 35 °C to 600 °C with a heating rate of 10 °C/min.

### 3.5.5 X-ray Diffraction (XRD)

XRD patterns of samples were performed in an X-ray diffractometer (XRD) instrument (RINT2000, Rigaku) using Cu K $\alpha$ 1 radiation ( $\lambda = 0.154$  nm) and a power of 40 kV and 20 mA. Samples were tested with a scanning angle of  $2\theta$  from 10° to 50° at a rate of 1°/min. The crystallinity index (CI) was calculated as a function of the maximum intensity of the diffraction peak from the crystalline region ( $I_{200}$ ), at an angle of  $2\theta \sim 22.5^\circ$ , and the minimum intensity from the amorphous region ( $I_{am}$ ), at an angle of  $2\theta \sim 18^\circ$ , according to the following equation<sup>64</sup>:

$$CI(\%) = \frac{I_{200} - I_{am}}{I_{200}} 100$$

## CHAPTER IV

### RESULTS AND DISCUSSION

#### 4.1 Purification of pineapple leaf fiber (PALF)

##### 4.1.1 Physical changes in PALF after purification treatment

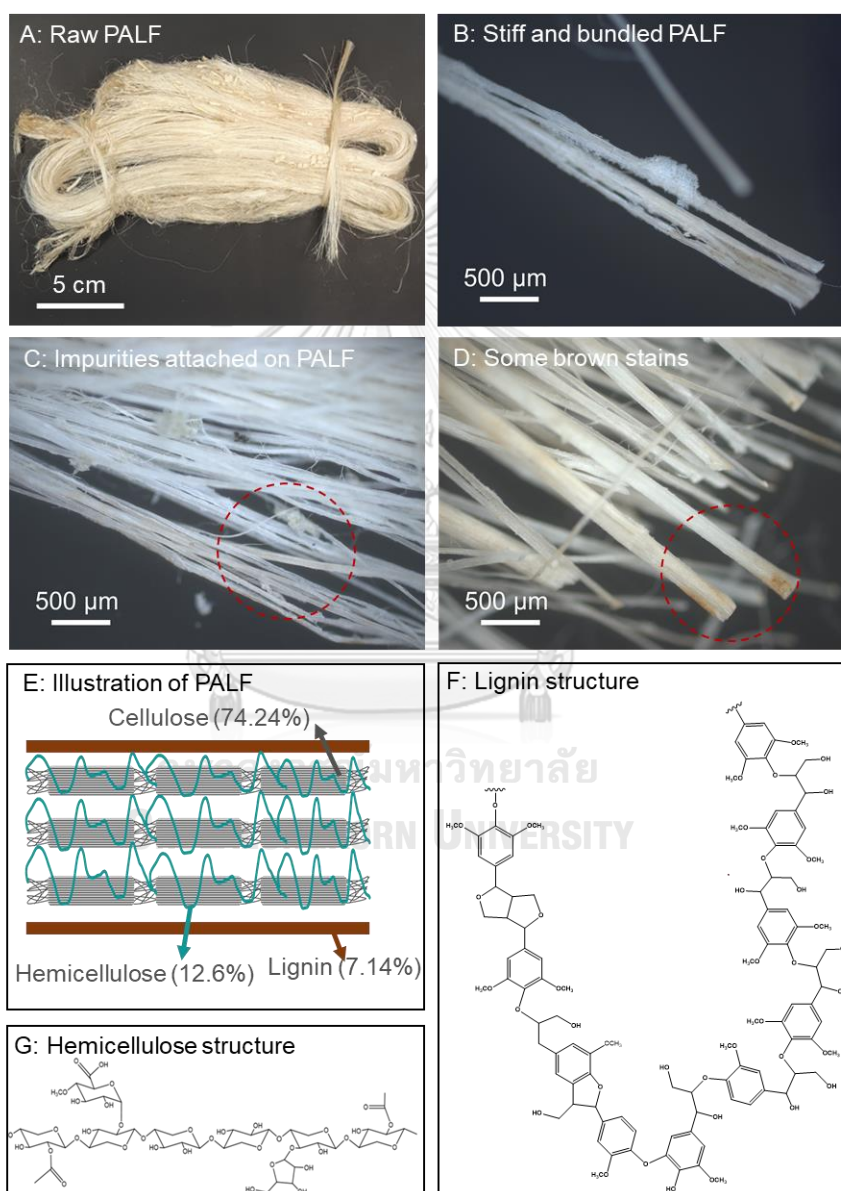


Figure 4.1 (A) Photographic image and (B-D) OM images of raw PALF, (E) drawing illustration of composite-like structure between cellulose, lignin, and hemicellulose in PALF, (F) lignin structure, and (G) hemicellulose structure.

Pineapple leaf fiber (PALF) was an abundant renewable raw material due to the huge production and consumption of pineapple fruit in Thailand, as we mentioned before. In this research, the raw PALF was supplied from local farmers in Thailand. The raw PALF has a length of ~90 cm with brown colour, stiff fiber, and impurities attached to its surface (Figure 4.1). Raw PALF is protected with lignin, cellulose, and hemicellulose, bundled together formed a rigid composite-like structure, made the PALF stiff and rigid<sup>39</sup>. The composite-like structure of PALF is illustrated in Figure 4.1E. Lignin had a complex polymer structure consisted of aryl ether and carbon-carbon linkages, which made the lignin hard to break<sup>65</sup> (Figure 4.1F). The brown colour in PALF was also one of the effects of lignin presence in PALF<sup>66</sup>. Compared to lignin, hemicellulose can be easily removed due to its structure that branches with short lateral chains, not as complex as lignin<sup>67</sup>.

The rigid composite-like structure of PALF formed by lignin and hemicellulose covering cellulose is the main obstacle to obtain the desired product in sulfuric acid treatment. Lignin and hemicellulose obstructed the sulfuric acid access to penetrate inside the PALF and possibly caused an undesired product<sup>22</sup>. In other words, purification treatment needed to be done to remove lignin and hemicellulose from PALF before treating it with sulfuric acid.

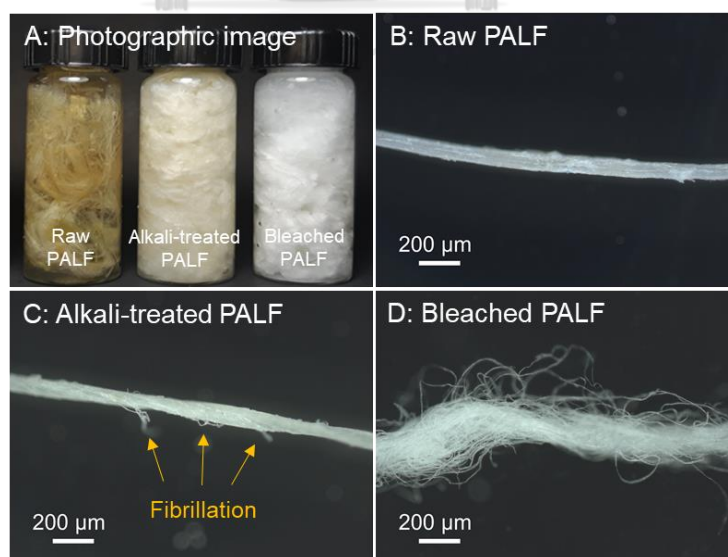


Figure 4.2 (A) Photographic image and (B-D) OM images of raw PALF, alkali-treated PALF, and bleached PALF.

Alkali and bleaching treatments as purification treatments were employed for PALF. In alkali treatment, the most commonly used alkali reagents are the hydroxyl derivatives of sodium, potassium, calcium, and ammonium salts. In this project, we used sodium hydroxide (NaOH) as an alkali reagent because NaOH has found to be most effective reagent among these hydroxyl derivatives, as mentioned in the previous research<sup>68</sup>. In the pretreatment process, the raw PALF was cut into ~10 cm lengths to make NaOH effectively penetrate to the PALF. After 2 hours, the solution became yellow. Meanwhile, the PALF turned out to be brighter. The change of colour in PALF after alkali treatment is displayed in Figure 4.2A. These results suggested that the lignin dissolution occurred. OM images (Figure 4.2B-C) that captured the structural change in the PALF have supported this statement. The raw PALF that was rigid and glued has started to show fibrillation, indicating that some fibers have freed. Alkali treatment cleaved the  $\beta$ -O-4 aryl ether bonds in lignin, which ~50-65% of lignin structure is  $\beta$ -O-4 aryl ether bond<sup>69</sup>. The cleavage of the  $\beta$ -O-4 aryl ether bond led to the destruction of the lignin structure. Figure 4.3 showed the cleavage reaction of the  $\beta$ -O-4 aryl ether bond in lignin during alkali treatment.

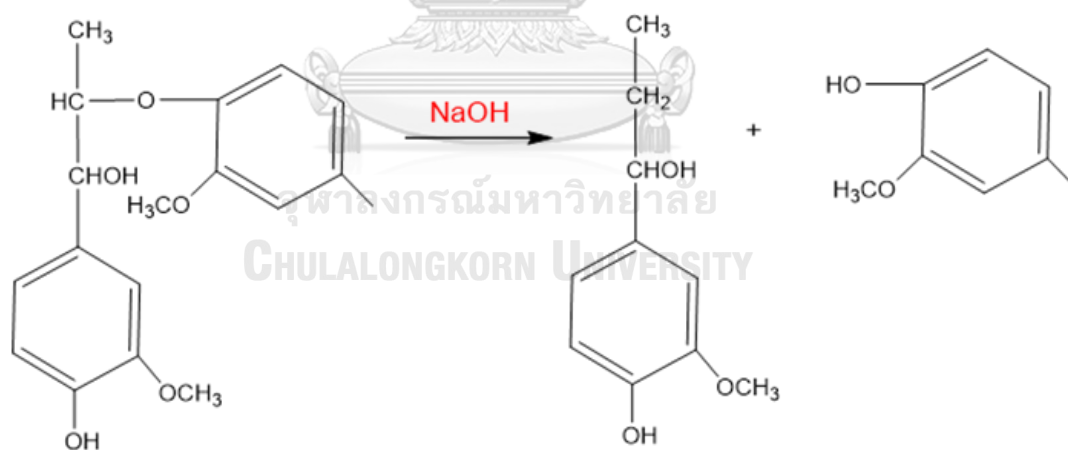


Figure 4.3 The cleavage reaction of the  $\beta$ -O-4 aryl ether bond in lignin during alkali treatment<sup>30</sup>.

However, observing from OM and photographic image, PALF were not entirely separated, and some brown colour still remained in fibers after alkali treatment. These results suggested that further purification treatment was required to wholly removed the lignin. Therefore, hydrogen peroxide ( $\text{H}_2\text{O}_2$ ) was applied to remove the lignin

residue in bleaching treatment. The advantages of bleaching using  $\text{H}_2\text{O}_2$  are low investment and strong bleaching effect<sup>28</sup>. Bleaching treatment was performed in the alkali condition (pH 10-12). In alkali media, the equilibrium of  $\text{H}_2\text{O}_2$  shifted to the formation of perhydroxyl anion ( $\text{HO}_2^-$ ) to be an active species to degrade the lignin from the fibers<sup>70</sup>. The reaction of  $\text{H}_2\text{O}_2$  activation in Figure 4.4 is shown.

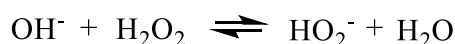


Figure 4.4 The reaction of  $\text{H}_2\text{O}_2$  activation in alkali condition<sup>71</sup>.

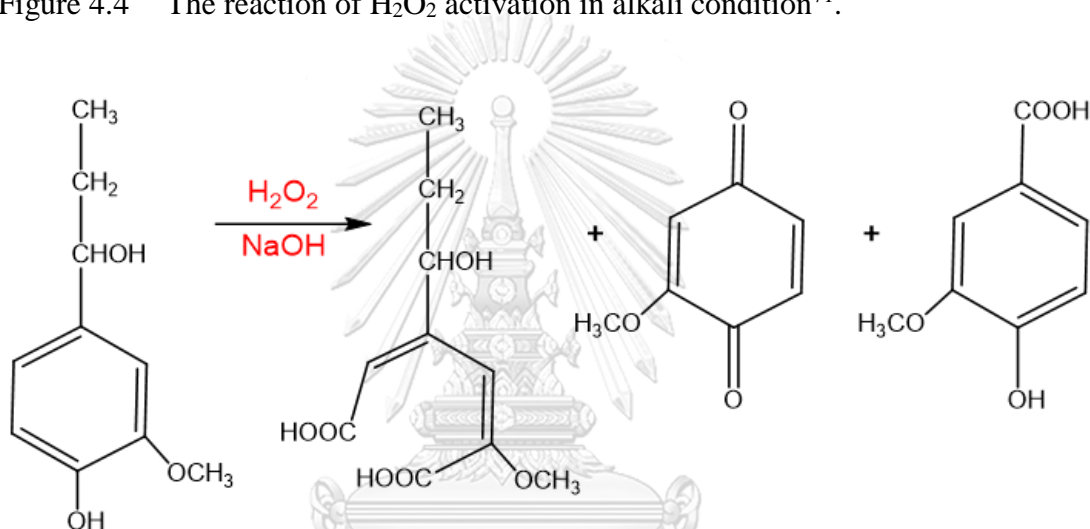


Figure 4.5 The reaction of the phenolate groups in lignin was oxidized into carboxylate in bleaching treatment<sup>72</sup>.

$\text{H}_2\text{O}_2$  oxidized the phenolate groups in the lignin structure and introduced the carboxylate group<sup>39, 70</sup>. The presence of carboxylate groups would increase the solubility of lignin in the water. The reaction of phenolate groups was oxidized into carboxylate in the bleaching treatment was explained in Figure 4.5. The perhydroxyl anion ( $\text{HO}_2^-$ ) oxidized the phenolate groups through ring-opening reaction, produced carboxylate, and led to the lignin dissolution<sup>72, 73</sup>.

The most noticeable change of PALF after bleaching treatment was the fibers that happened to be white. We mentioned before that the lignin gave brown colour to the fibers (Figure 4.1A). In other words, the white colour on PALF can be a preliminary indicator of the lignin residue removal. The structural change of PALF

after bleaching treatment has been observed from OM images in Figure 4.2D. The PALF was no longer intact and separated into small fibers, designating that the rigid composite-like structure between cellulose, lignin, and hemicellulose has destructed.

#### 4.1.2 Chemical structural changes in PALF after purification treatment

FT-IR spectroscopy was used for obtaining molecular information on chemical structural changes taking place in PALF during purification treatment. The band assignments of F-TIR spectra in Figure 4.6 are shown in Table 4.1.

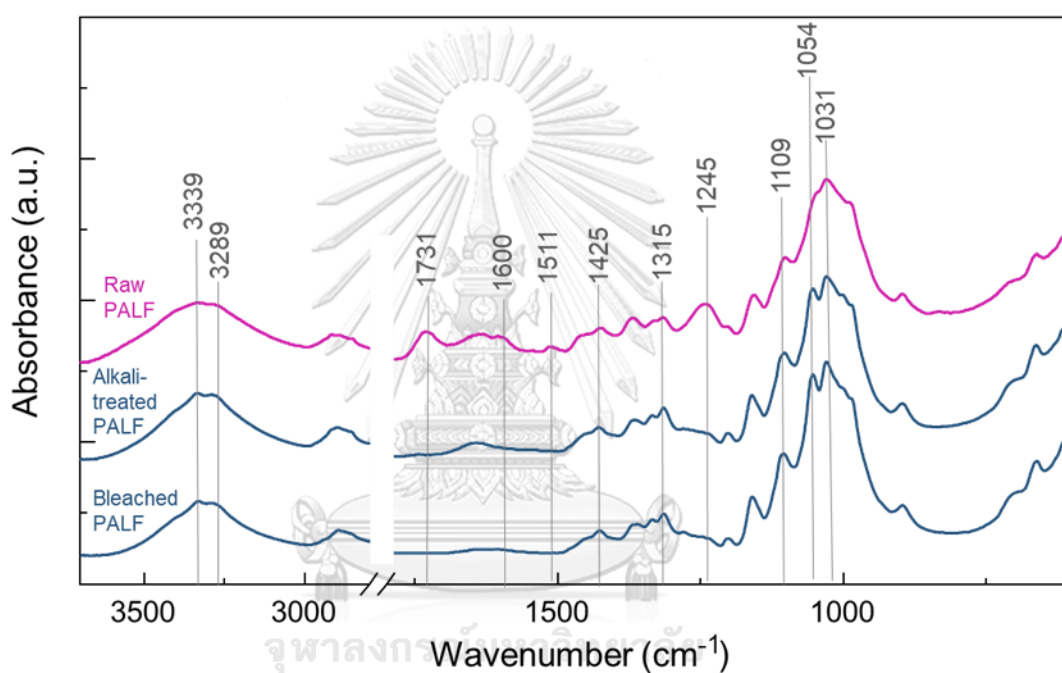


Figure 4.6 FT-IR spectra of raw PALF, alkali-treated PALF, and bleached PALF.

Table 4.1 Band assignments of FT-IR spectra raw, alkali-treated, and bleached PALF.

Wavenumber (cm <sup>-1</sup> )	Vibrational Mode	Band assignment	Compound	Reference
3339	$\gamma$ OH	OH stretching of intramolecular H-bonding at O(3)H $\cdots$ O(5)	Cellulose	74-77
3289	$\gamma$ OH	OH stretching of intermolecular H-bonding at O(6)H $\cdots$ O'(3)H	Cellulose	77
1731	$\gamma$ C=O	C=O stretching in unconjugated ketones aldehydes and carboxyl	Hemicellulose	7, 78-80
1600	$\gamma$ C=C	C=C stretching of the aromatic ring	Lignin	78, 80
1511	$\gamma$ C=C	C=C stretching of the aromatic ring	Lignin	77, 78, 80
1315	$\delta$ CH <sub>2</sub>	CH <sub>2</sub> wagging of C(6)	Cellulose	74, 78
1245	$\gamma$ CO	CO stretching of acetyl groups	Lignin and hemicellulose	12, 77, 78
1109		CO valence vibration of C(3)-O(3)H	Cellulose	74, 75
1054	$\gamma$ CO	CO stretching of C(6)	Cellulose	74, 75
1031	$\gamma$ CO	CO stretching of C(6)	Cellulose	74, 75, 81

Notes:  $\gamma$ : stretching,  $\delta$ : bending.

FT-IR spectra of PALF showed some changes after the purification treatment. The first observable change was the disappearance of peaks at 1731, 1600, 1511, and 1245 cm<sup>-1</sup>. These peaks attributed to the carbonyl group (C=O) stretching in hemicellulose, C=C stretching of the aromatic ring in lignin, and CO stretching of acetyl groups in lignin and hemicellulose, respectively<sup>77, 80</sup>. This result indicated that hemicellulose and lignin were removed.

As the interferences were removed from the PALF, some peaks corresponding to the cellulose content have become more prominent. Peaks at 3339 and 3289 cm<sup>-1</sup>, which representing OH stretching of intramolecular H-bonding at O(3)H $\cdots$ O(5) and intermolecular H-bonding at O(6)H $\cdots$ O'(3)H, respectively, belonged to cellulose have become more pronounced. Lignin and hemicellulose also had inter and intramolecular H-bonding. This bonding disturbed the absorption intensity of inter and intramolecular H-bonding in cellulose. While the lignin and hemicellulose have been

removed, the absorption intensity of inter and intramolecular H-bonding in cellulose became more visible<sup>82</sup>. Peaks at  $1315\text{ cm}^{-1}$  associating with  $\text{CH}_2$  wagging of C(6) have increased significantly after purification treatment due to the increment of crystalline content in cellulose, which is also related to the shifted peak  $1425\text{ cm}^{-1}$ <sup>78, 82</sup>. The increment of the peak at  $1109\text{ cm}^{-1}$  representing CO valence vibration of C(3)-O(3)H is associated with the more prominent peaks at  $3289$  and  $3339\text{ cm}^{-1}$ . The peak at  $1054$  and  $1031\text{ cm}^{-1}$ , attributing to CO stretching of C(6). These peaks have significantly increased due to the cleavage of lignin that connected with the cellulose at C(6). The bond at C(6)-O has freed from the lignin and increased the absorption intensity of the spectra<sup>83</sup>. The FT-IR spectra between alkali-treated PALF and bleached PALF were similar, suggesting that the amount of lignin residue was too small to be detected in spectra. Peaks at  $1054$  and  $1031\text{ cm}^{-1}$  have slightly increased in bleached PALF due to removing lignin residue that interfered with the CO bonding of cellulose before.

Overall, FT-IR spectra are in good agreement with those reported in the literature for other plant cellulose and with the previous results of structural images<sup>7, 12, 23, 84</sup>. We can conclude that the purification treatment has successfully removed the hemicellulose and lignin, obtaining pure cellulose.

#### 4.1.3 Comparison of bleached PALF with commercial cellulose standards

In the previous section, we have demonstrated that the purification has successfully done to remove the impurities from PALF. To be more sure about the cleanness of our bleached PALF, we tried to compare our bleached PALF with the commercial cellulose standards, which are filter paper, Kim-Tech wipes, Avicel PH101, and bacterial cellulose (BC).

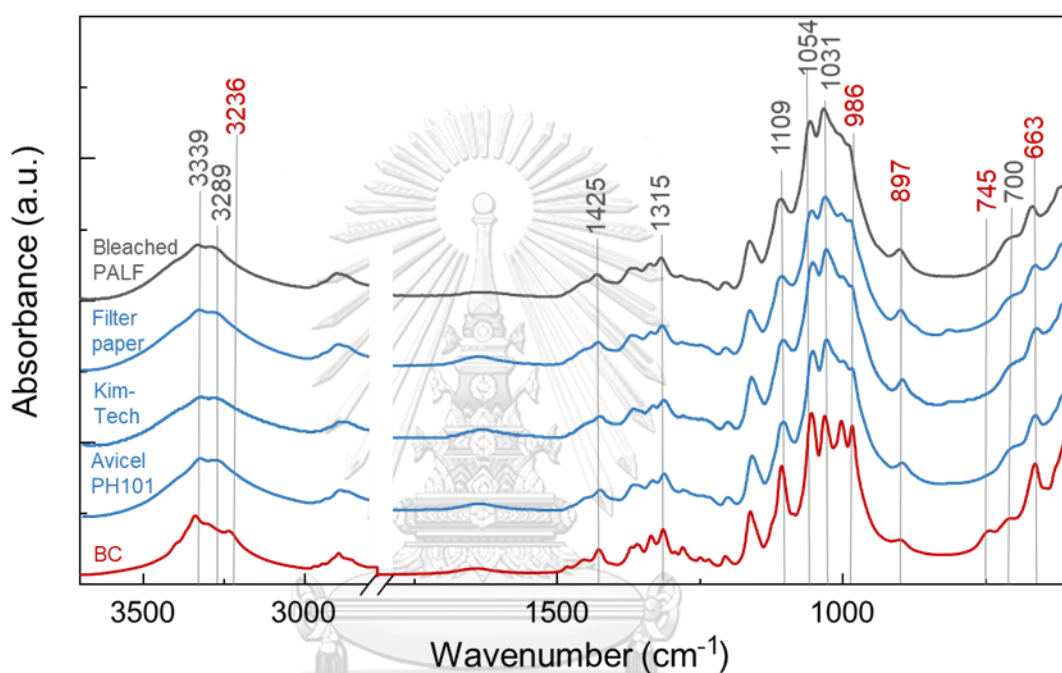


Figure 4.7 FT-IR spectra of bleached PALF, filter paper, Kim-Tech, Avicel PH101, and bacterial cellulose (BC).

The four spectra of bleached PALF, filter paper, Kim-Tech, and Avicel PH101 have the same pattern, as shown in Figure 4.7. Peaks corresponding to lignin and hemicellulose in four spectra have not appeared (2850, 1731, 1600, 1513, and 1245  $\text{cm}^{-1}$ ), indicating that the impurities have not existed in all samples<sup>23</sup>. In OH region, peaks at 3339 and 3289  $\text{cm}^{-1}$  that we mentioned before belonged to inter and intramolecular H-bonding of cellulose shown as prominent as the filter paper, Kim-Tech, and Avicel PH101. Peaks at 1315, 1109, 1054, and 1031  $\text{cm}^{-1}$ , sensitive to the cellulose content, have the same intensity<sup>78, 82</sup>. These results suggested that the bleached PALF was already cleaned.

It is also worth noting that the same pattern of bleached PALF, filter paper, Kim-Tech, and Avicel PH101 due to the same source of cellulose, which is plant cellulose. The cellulose from plant predominantly produced cellulose type allomorphs I $\beta$ <sup>85</sup>. Meanwhile, I $\alpha$  is mainly made by BC<sup>86</sup>. We compared our bleached PALF with BC to observe the difference between I $\beta$  and I $\alpha$ . BC also can be an excellent comparison to prove the cleanness of PALF since BC did not contain any lignin and hemicellulose because of it obtained from the bacterial<sup>87</sup>. Band assignments attributing to the bleached PALF and BC FT-IR spectra are listed in Table 4.2.

Table 4.2 Band assignments of FT-IR spectra from bleached PALF and BC.

Wavenumber (cm <sup>-1</sup> )	Vibrational Mode	Band assignment	Compound	Reference
3339	$\gamma$ OH	OH stretching of intramolecular H-bonding at O(3)H $\cdots$ O(5)	I $\beta$ , I $\alpha$	74-77
3289	$\gamma$ OH	OH stretching of intermolecular H-bonding at O(6)H $\cdots$ O'(3)H	I $\beta$	77
3236	$\gamma$ OH	OH stretching of intermolecular H-bonding at O(6)H $\cdots$ O'(3)H	I $\alpha$	86
1425	$\delta$ CH <sub>2</sub>	CH <sub>2</sub> scissoring of C(6)	I $\beta$ , I $\alpha$	74, 75, 78
1315	$\delta$ CH <sub>2</sub>	CH <sub>2</sub> wagging of C(6)	I $\beta$ , I $\alpha$	74, 78
1109		CO valence vibration of C(3)-O(3)H	I $\beta$ , I $\alpha$	74, 75
1054	$\gamma$ CO	CO stretching of C(6)	I $\beta$ , I $\alpha$	74, 75
1031	$\gamma$ CO	CO stretching of C(6)	I $\beta$ , I $\alpha$	74, 75, 81
897	$\gamma$ COC	C-O-C stretching symmetric of glycosidic linkage	I $\beta$ , I $\alpha$	74, 75
745	$\delta$ OH	OH bending out of plane	I $\alpha$	88
700	$\delta$ OH	OH bending out of plane	I $\beta$	88
663	$\gamma$ CO	COH bending out of plane	I $\beta$ , I $\alpha$	74, 75, 81

Notes:  $\gamma$ : stretching,  $\delta$ : bending.

The apparent difference of FT-IR spectra between bleached PALF (I $\beta$ ) and BC (I $\alpha$ ) was at OH region (3500-3000 cm<sup>-1</sup>) because the difference between I $\beta$  and I $\alpha$  was their three-dimensional (3D) crystal form and the inter and intramolecular H-bonding formed their 3D crystals<sup>86, 89</sup>. The peak attributing to OH stretching of intermolecular H-bonding at O(6)H $\cdots$ O' (3)H was at a different characteristic position. The position

of  $I_{\beta}$  was at  $3289\text{ cm}^{-1}$ , while for  $I_{\alpha}$  was at  $3236\text{ cm}^{-1}$ <sup>89</sup>. The peak of BC at  $3339\text{ cm}^{-1}$  representing OH stretching of intramolecular H-bonding at  $\text{O}(3)\text{H}\cdots\text{O}(5)$  has a higher intensity compared to bleached PALF. This high intensity happened due to the characteristic of BC that has high crystallinity and purity in its cellulose. Furthermore, the peak attributing to OH bending out of plane for  $I_{\alpha}$  ( $745\text{ cm}^{-1}$ ) and  $I_{\beta}$  ( $700\text{ cm}^{-1}$ ) also in a different position. Yu et al. (2013) mentioned that the different peak positions of OH occurred due to the different strength of H-bonding in  $I_{\alpha}$  and  $I_{\beta}$ <sup>88</sup>. Other peaks corresponding to the cellulose content ( $1425$ ,  $1315$ ,  $1109$ ,  $1054$ ,  $1031$ , and  $663\text{ cm}^{-1}$ ) of  $I_{\alpha}$  and  $I_{\beta}$  were at the same position, distinct only at the intensity, as a consequence of different resource<sup>90</sup>.

As our bleached PALF has the same intensity and pattern as all commercial cellulose standards, we concluded that the pure cellulose has already been obtained from our bleached PALF. The  $I_{\beta}$  and  $I_{\alpha}$  were chemically identical but differ in the 3-D crystal arrangements of cellulose chains in the unit cell that made some peak position not the same. After we confirmed that we obtained pure cellulose from bleached PALF, the bleached PALF was ready to use for the next treatment, which was sulfuric acid treatment.

#### 4.1.4 Thermal properties of PALF

Wet tried to investigate the effect of removing lignin and hemicellulose in the thermal properties of the PALF samples. The thermal properties of PALF were observed using thermogravimetric analysis (TGA), which involved analyzing the weight loss of the sample as a function of temperature<sup>91</sup>.

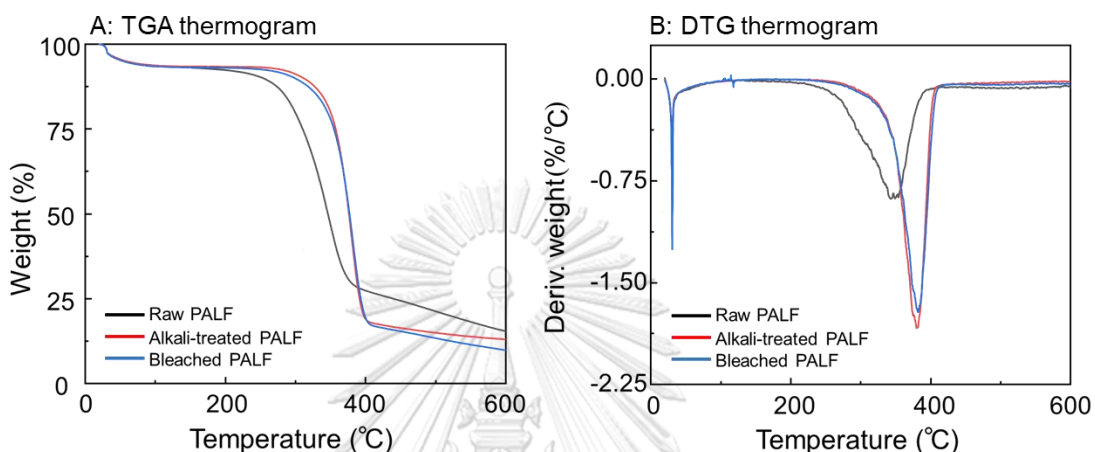


Figure 4.8 (A) TGA and (B) DTG thermograms of raw PALF (black), alkali-treated PALF (red), and bleached PALF (blue).

Table 4.3 Thermal properties profiles of raw PALF, alkali-treated PALF, and bleached PALF.

Samples	Onset T (°C)	Decomposition T (°C)	Weight loss at 600 °C (%)
Raw PALF	288	342	85.1
Alkali treated PALF	344	380	86.8
Bleached PALF	340	382	90.0

TGA thermograms and its derivatives (DTG) of the raw, alkali-treated, and bleached PALF have been displayed in Figure 4.8. The onset temperature, decomposition temperature, and percentage weight loss at 600 °C have listed in Table 4.3. It found that all samples exhibited a one-step degradation process. The weight loss below 100 °C was attributed to water evaporation. The primary degradation of raw PALF has started at 288 °C and got maximum decomposition temperature at 342 °C. It has been observed that there is a significant increment in the thermal properties

profile of PALF after applying purification treatment. The onset and decomposition temperatures of PALF have shifted to 340°C and 382 °C, respectively. The lignin and hemicellulose trace has disappeared from previous FT-IR spectra, which confirmed lignin and hemicellulose removal after purification treatment. Combining this result, we suggested that the increment of thermal properties has related to lignin and hemicellulose removal. The increment of thermal properties due to lignin and hemicellulose removal has also been reported in previous works of Santos et al. (2013) and Zhou et al. (2017)<sup>7, 92</sup>. Our results are also in good agreement with Kim et al. (2006) that said hemicellulose mainly degraded at 150-350 °C, cellulose at 275-350 °C, and lignin at 250-500 °C, which mean that hemicellulose and lignin possibly take degradation faster than cellulose<sup>93</sup>.

The TGA and DTG results confirmed that lignin and hemicellulose made the thermal properties of PALF degraded. By removing lignin and hemicellulose from PALF, better thermal properties would be obtained, which can be used to assess its potential value in high-temperature applications<sup>91</sup>.

#### 4.2 PALF in 25% H<sub>2</sub>SO<sub>4</sub> (sulfuric acid) treatment

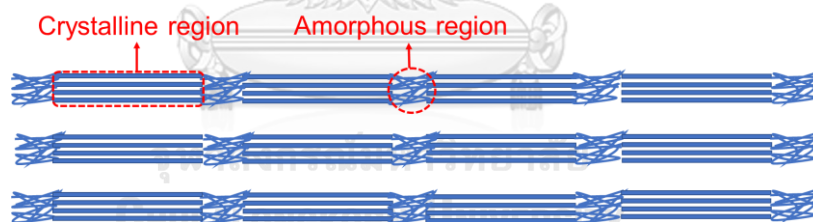


Figure 4.9 Drawing illustration of cellulose structure in bleached PALF consists of amorphous and crystalline regions.

In the previous FT-IR spectra of bleached PALF, we have confirmed that our bleached PALF had no lignin and hemicellulose left. The rigid composite-like structure formed by lignin, cellulose, and hemicellulose has broken down, remaining the cellulose. The cellulose itself consisted of the amorphous and crystalline regions in its structure, illustrated in Figure 4.9<sup>94</sup>. The crystalline region has an order arrangement structure of strong inter and intramolecular H-bonding held firmly together side-by-side<sup>95</sup>. The main objective of this research is to develop a process to

obtain regenerated amorphous cellulose (RAC). To accomplish this aim, we need to dissolve the native cellulose. But due to its strong inter and intramolecular H-bonding, the cellulose would be hard to process in conventional solvents such as water or ethanol<sup>95</sup>. To produce our RAC, we have to treat cellulose using sulfuric acid (H<sub>2</sub>SO<sub>4</sub>) as a solvent.

Huang et al. (2016) first reported using 64% (v/v) H<sub>2</sub>SO<sub>4</sub> at low temperature (-20 °C) to obtain RAC<sup>17</sup>. Interestingly, Santos et al. (2013) using the same acid concentration at high temperature (45 °C), producing a very different product, which is nanocrystalline cellulose (NCC)<sup>7</sup>. It is safe to say that temperature treatment is playing an essential role in obtaining RAC and NCC.

Many works have focused on research using a high acid concentration (more than 60% H<sub>2</sub>SO<sub>4</sub>) in producing cellulosic products<sup>7, 17, 96</sup>. Apparently, the behavior of cellulose products obtaining in low acid concentrations and different temperatures has not been particularly observed. In this section, we tried to investigate the influence of using low acid concentration (25% v/v H<sub>2</sub>SO<sub>4</sub>) at different temperature sulfuric acid treatment (-20, 30, and 50 °C) by following the physical, chemical structure, and thermal properties of PALF after sulfuric acid treatment.

#### **4.2.1 Physical properties of PALF after 25% (v/v) sulfuric acid treatment**

Morphology of PALF after sulfuric acid treatment was observed using an optical microscope (OM) with a corresponding histogram of length and width distributions. Figure 4.10A showed that the bleached PALF initially has long fibers entangled together. The long fibers have spread into short fibers with various lengths and widths after sulfuric treatment, depending on its temperature treatment (Figure 4.10B-D). Bleached PALF and short fibers were characterized by their length (L), width (D), and aspect ratio (L/D). A minimum of 300 particles has been used to measure the length and width of short fibers. The average diameter, length, and aspect ratio were listed in Table 4.4.

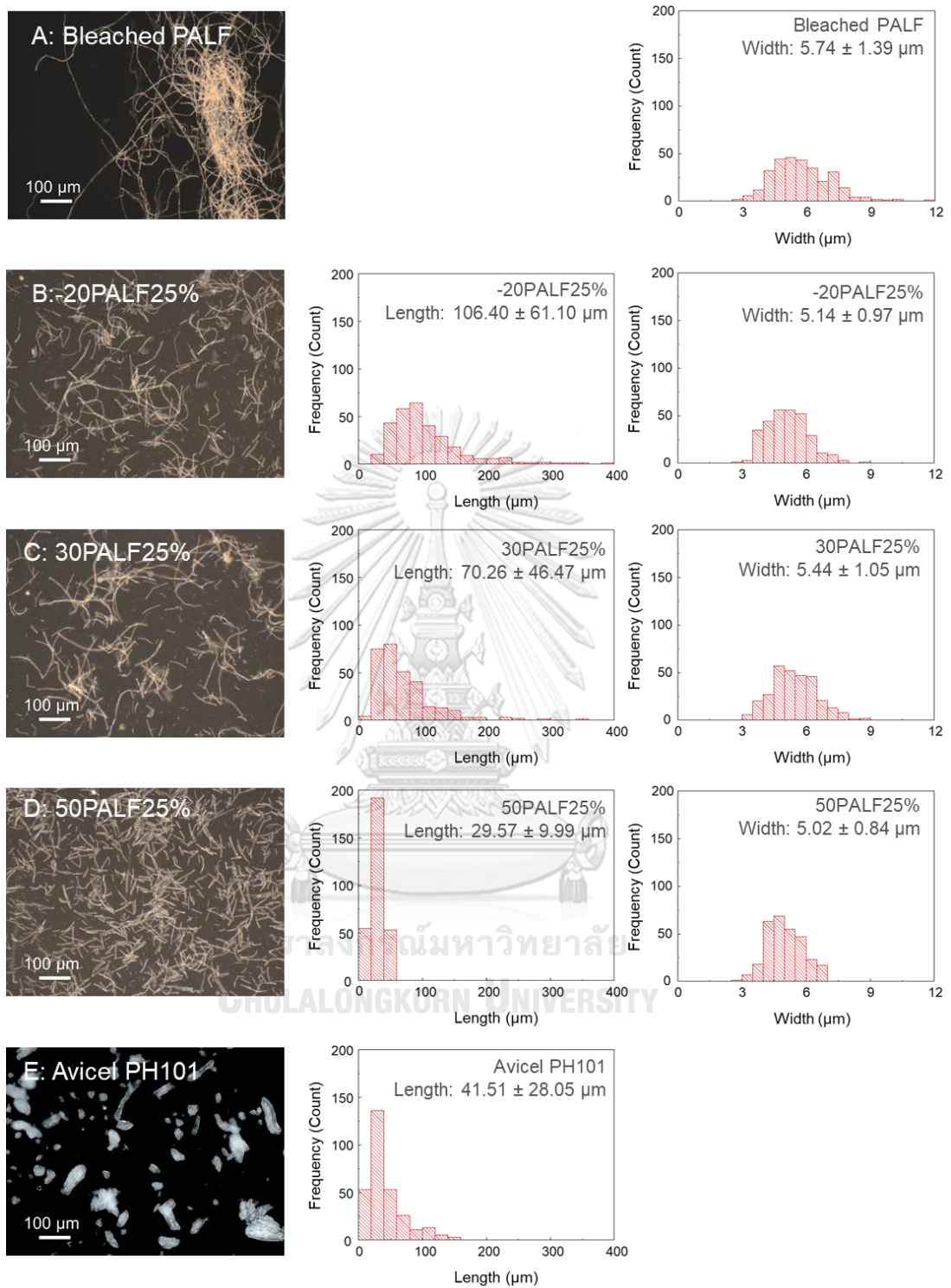


Figure 4.10 OM images of (A) bleached PALF, (B) -20PALF25%, (C) 30PALF25%, (D) 50PALF25%, and (E) Avicel PH101 and corresponding size distribution.

Table 4.4 Average diameter (D), length (L), and aspect ratio (L/D) of bleached PALF, short fibers after sulfuric acid treatment, and Avicel PH101.

Samples	L ( $\mu\text{m}$ )	D ( $\mu\text{m}$ )	L/D
Bleached PALF	-	$5.74 \pm 1.39$	-
-20PALF25%	$106.40 \pm 61.10$	$5.14 \pm 0.97$	21
30PALF25%	$70.26 \pm 46.47$	$5.44 \pm 1.05$	13
50PALF25%	$29.57 \pm 9.99$	$5.02 \pm 0.84$	6
Avicel PH101	$41.51 \pm 28.05$	-	-

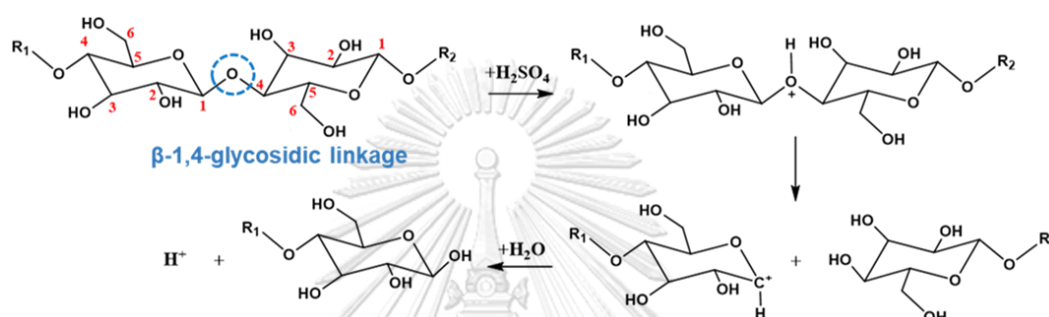


Figure 4.11 The reaction of hydrolysis in sulfuric acid treatment.

Bleached PALF has a width of  $5.74 \pm 1.39 \mu\text{m}$  with undetermined length due to its entangled long fibers, possibly length in the centimeters range. Meanwhile -20PALF25%, 30PALF25%, and 50PALF25%, have length and width about  $106.40 \pm 61.10$  and  $5.14 \pm 0.97$ ,  $70.26 \pm 46.47$  and  $5.44 \pm 1.05$ ,  $29.57 \pm 9.99$  and  $5.02 \pm 0.84 \mu\text{m}$ , respectively, categorized as microcrystalline cellulose (MCC)<sup>45, 97, 98</sup>. The MCC was well-known formed by a partial hydrolysis reaction<sup>97, 99</sup>. The hydrolysis in sulfuric acid happened when hydronium ions ( $\text{H}^+$ ) from acid attach to the  $\beta$ -1,4-glycosidic bonds, causing a split in the cellulose chain. The formed carbonium ion reacts with a water molecule, which liberates an  $\text{H}^+$ <sup>17, 100</sup>. The reaction of hydrolysis was written in Figure 4.11.

In hydrolysis, the amorphous region in cellulose would be more affected and removed because acid could easily access the amorphous glycosidic bonds due to its less ordered form. Meanwhile, the crystalline region ordered form would make the acid hard to penetrate through the crystalline region. In partial hydrolysis, the amorphous removal is not intensive, made some amorphous regions was indelible and remained in the cellulose. This condition made the amorphous intact together with the

crystalline region, forming a micro-size material called microcrystalline cellulose (MCC)<sup>101</sup>. The illustration of partial hydrolysis that happened during forming MCC was displayed in Figure 4.12.

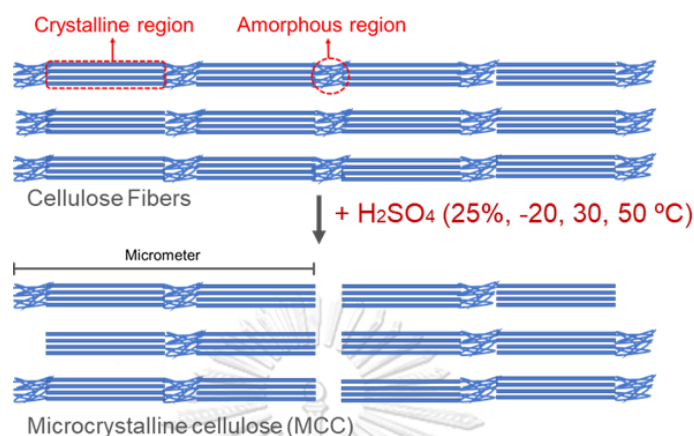


Figure 4.12 Drawing illustration of partial hydrolysis occurred, forming microcrystalline cellulose (MCC).

A significant length reduction could be seen from -20PALF25%, 30PALF25%, and 50PALF25% compared to bleached PALF (Table 4.4). By increasing the treatment temperature, the shorter MCC has been obtained. Similar results have been reported by Tan (2015), suggesting that as the treatment temperature was increased, hydronium ions penetrated the more accessible amorphous regions at a higher rate during the hydrolysis and subsequently cleaved the glycosidic bonds, obtaining shorter MCC<sup>102</sup>. In contrast, the decrement of the width happened slightly (decreased about 5-12.5%). These phenomena are related to the crystalline region's ability to be less affected in the hydrolysis reaction than the amorphous region<sup>18, 51</sup>. The amorphous and crystalline regions in PALF were located on the surface and their main axis<sup>97</sup>. As shown in Figure 4.12, the amorphous region contributed to arranging the length axis of PALF. Meanwhile, the crystalline region established width axis<sup>97</sup>. It was mentioned before that the amorphous region had been affected more than the crystalline region. So, when the hydrolysis occurred, the amorphous region was intensively removed, the crystalline region was only slightly defective, resulting in a significant length reduction and mild width reduction.

Besides, the uniformity in the length of MCC PALF also increased significantly with the temperature increment. The standard deviation reported for the length of - 20PALF50%, 30PALF50%, and 50PALF50% were  $\pm 61.10$ ,  $\pm 46.47$ , and  $\pm 9.99$   $\mu\text{m}$ , respectively, as a parameter of uniformity. These findings indicated that more homogeneous MCC could be obtained by increasing the treatment temperature. This trend was not obvious for the width.

The physical properties of our MCC were compared with a commercially available MCC Avicel PH101. As mentioned before, our MCC has a short fiber shape. On the other hand, Figure 4.10E showed the morphology of Avicel PH101 with an irregular shape<sup>103</sup>. The average length for the Avicel PH101 particles was  $41.51 \pm 28.05$   $\mu\text{m}$  with undetermined width attributing to its irregular shape. The morphology difference between our MCC and Avicel PH101 because Avicel PH101 came from a wood source, while our MCC was PALF<sup>98</sup>. Moon et al. (2011) reported that the morphology of cellulose depended on the source of the original cellulose<sup>40</sup>.

Due to the irregular shape of Avicel PH101, its aspect ratio could not be measured. It is well known that MCC's aspect ratios played a crucial role in most of their applications, such as pharmaceutical tablets application<sup>104</sup>. Another property that important was uniformity. The uniformity of 50PALF25% was also more eminent compared to Avicel PH101 showed from their standard deviation. Our MCC offers a definite advantage over Avicel PH101 in the aspect ratio and uniformity. Our MCC could also be a potential alternative in producing a commercial MCC based on its simple process and ability to control the size.

#### 4.2.2 Chemical structural changes of PALF in 25% (v/v) H<sub>2</sub>SO<sub>4</sub>

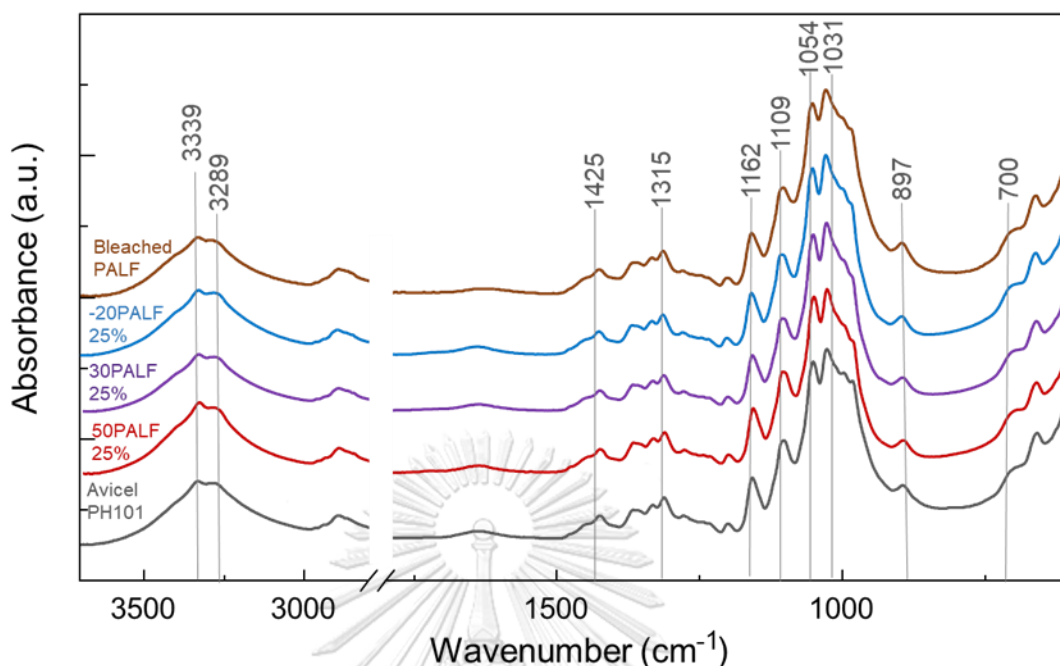


Figure 4.13 FT-IR spectra of bleached PALF, -20PALF25%, 30PALF25%, 50PALF25%, and Avicel PH101 at 3900-600 cm<sup>-1</sup> region.

FT-IR spectroscopy is an appropriate technique to establish the variations introduced by low acid concentration and different temperature treatments on the chemical structure of the treated samples. FT-IR spectra of bleached PALF, -20PALF25%, 30PALF25%, 50PALF25%, and Avicel PH101 shown in Figure 4.3. All spectra exhibited almost similar profiles. The absence of additional peaks in the spectra of PALF after 25% sulfuric acid treatment indicated that all samples had there is no significant change of chemical structures in the process of hydrolysis<sup>105</sup>. A slightly narrower profile was found after acid treatment in all MCC PALF samples at peaks in the 3500–3000 cm<sup>-1</sup>, which correspond to OH stretching vibrations, suggesting that the hydrolysis process weakened the H-bonding of cellulose but not disrupt the arrangement<sup>106</sup>.

The same profile of FT-IR spectra in MCC PALF and Avicel PH101 suggested that even the morphology was different, but the chemical composition on their structure was the same. The same profile indicated the same cellulose type allomorph as well. The profile of these spectra representing cellulose I<sub>β</sub>. A confirmation that

MCC PALF and Avicel PH101 have cellulose  $I_{\beta}$  type was proved by the absence of the peak at  $745\text{ cm}^{-1}$ , which is the characteristic peak of cellulose  $I_{\alpha}$ <sup>88</sup>. The peak attributed to OH stretching of intermolecular H-bonding at  $O(3)H\cdots O'(6)H$  also appeared at  $3289\text{ cm}^{-1}$ , which is the characteristic peak of cellulose  $I_{\beta}$ <sup>86, 88</sup>.

From these results, it was noteworthy that the MCC obtained from PALF via sulfuric acid treatment is close to the commercial MCC.

#### 4.2.3 Thermal properties of bleached PALF and cellulosic products

Thermal properties of PALF after 25%  $H_2SO_4$  (sulfuric acid) treatment was investigated.

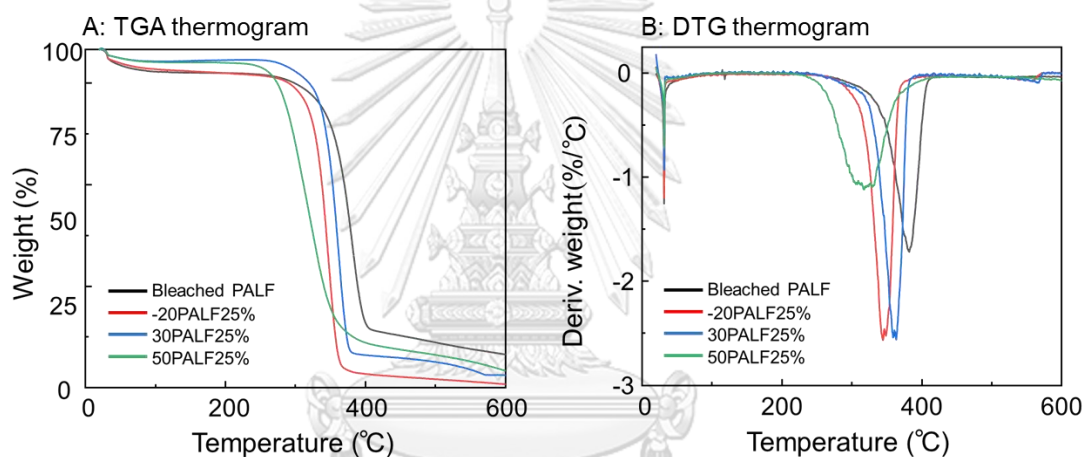


Figure 4.14 (A) TGA and (B) DTG thermograms of bleached PALF (black), -20PALF25% (red), 30PALF25% (blue), and 50PALF25% (green).

Table 4.5 Thermal properties profile of bleached PALF, -20PALF25%, 30PALF25%, and 50PALF25%.

Samples	Onset T (°C)	Decomposition T (°C)	Weight loss at 600 °C (%)
Bleached PALF	340	382	90.0
-20PALF25%	317	344	100.0
30PALF25%	332	364	96.2
50PALF25%	281	318	95.0

Figure 4.14 showed thermogravimetric analysis (TGA) and derivative thermograms (DTG) curves for bleached PALF, -20PALF25%, 30PALF25%, and

50PALF25%. Table 4.5 reported the data obtained from Figure 4.14. The TGA curves for all the samples showed two weight loss stages within the temperature of 50-600 °C. The drying stage for the samples occurred at a temperature below 100 °C, which was associated with the evaporation of water<sup>43</sup>. For bleached PALF, the main degradation started at 340 °C, suggesting the cellulose degradation processes, such as dehydration, decarboxylation, depolymerization, and decomposition of glycosyl units, followed by the formation of a charred residue<sup>107</sup>. After sulfuric acid, a decrement in degradation temperature compared to the bleached PALF was found. Sample -20PALF25%, 30PALF25%, and 50PALF25% have decrement of onset temperature about 23, 8, and 59 °C, respectively. This degradation behavior was also reported in previous researches on sulfuric acid treatment<sup>12, 18, 107</sup>. Vasconcelos et al. (2017) explained that the decrement of thermal properties in sulfuric acid-treated samples due to the presence of sulfate groups<sup>90</sup>. The presence of sulfate groups causes decreased activation energy for the thermal degradation of cellulose<sup>90, 108</sup>.

The degradation temperature of the sulfuric acid-treated samples comparing with each other has also been observed. The higher amount of sulfate groups in MCC would lead to a higher decreased degradation temperature in MCC<sup>48</sup>. On the other hand, the number of sulfate groups in cellulose is related to MCC size. The smaller size would lead to a higher surface area, which means more access to sulfate groups on the MCC surface<sup>109</sup>. The onset temperature of -20PALF25%, 30PALF25%, and 50PALF25% were started at 317, 332, and 281 °C, respectively. Related to the previous result of MCC's length, the degradation temperature of -20PALF25% and 50PALF25% were in the same agreement with the previous statement. But there is an anomaly on 30PALF25%, which has a higher degradation temperature than -20PALF25%. The effect of width decrement might be related to this phenomenon. We suggested that the size of width has more effect on the decrement of degradation temperature than the length because the defect of the crystalline region occurred in the width decrement. Due to the width decrement, the sulfate groups would attach less on the MCC.

### 4.3 PALF in sulfuric acid treatment of 50% (v/v) H<sub>2</sub>SO<sub>4</sub>

The influence of 50% (v/v) H<sub>2</sub>SO<sub>4</sub> and the temperature treatment (-20, 30, and 50 °C) on the physical, chemical structural, crystallinity, and thermal properties of PALF and its cellulosic products were investigated.

#### 4.3.1 Physical properties of PALF in 50% (v/v) H<sub>2</sub>SO<sub>4</sub>

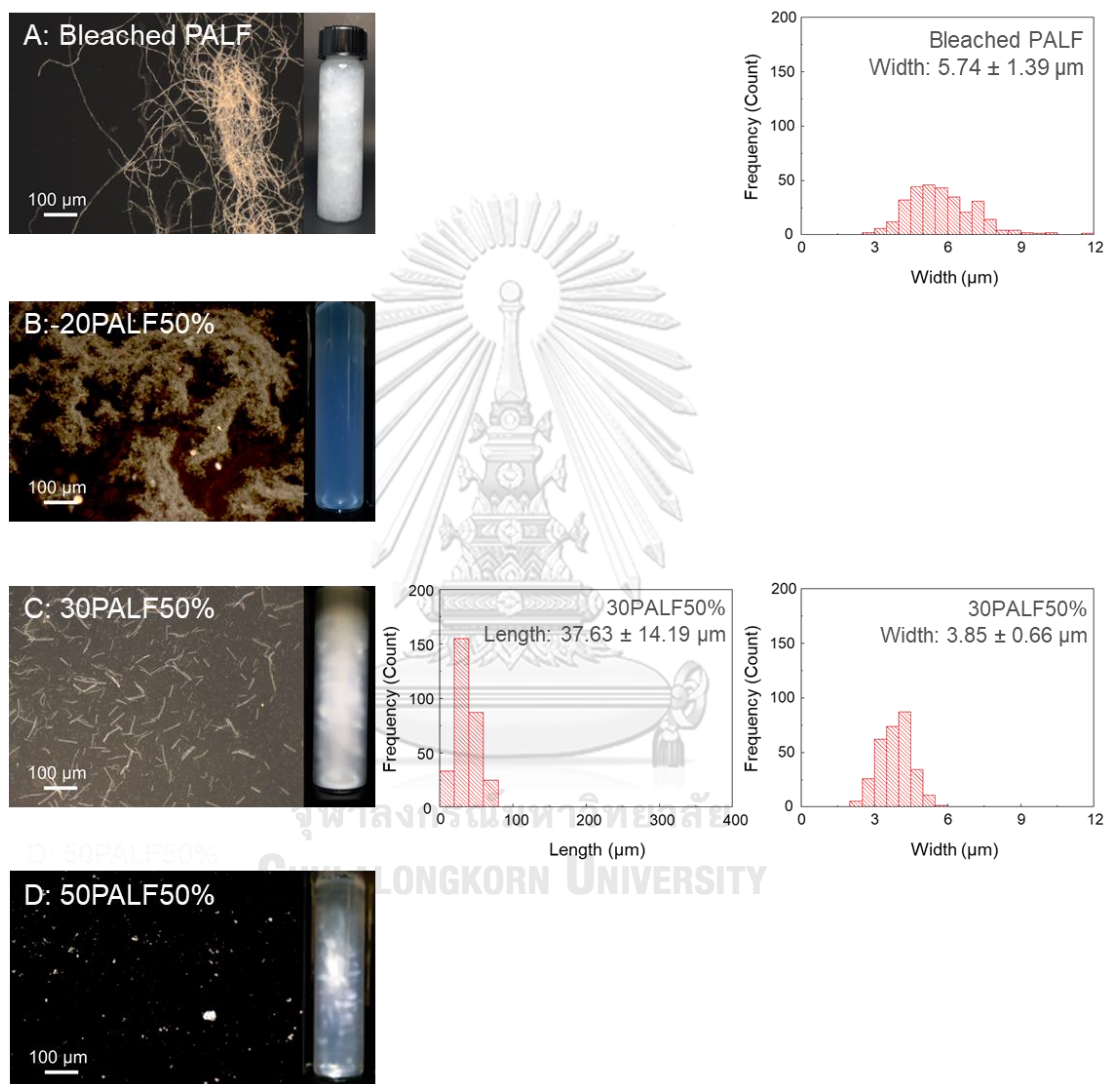


Figure 4.15 OM images of (A) bleached PALF, (B) -20PALF50%, (C) 30PALF50%, (D) 50PALF50%, cross-polarizer images, and corresponding size distribution of lengths and widths.

Figure 4.15 showed a series of OM images assisted with cross-polarizer images of a bleached PALF after sulfuric acid treatment at three different temperatures. The bleached PALF exhibited long fibers with a width of about  $5.74 \pm 1.39 \mu\text{m}$  and an

undetermined length due to its long fiber entangled. The morphology of the sample at each different temperature displayed a very different morphology. In -20PALF50%, the gel-like shape was captured by the OM image (Figure 4.15B). Jia et al. (2013) reported the gel-like shape of the cellulose is a characteristic of regenerated amorphous cellulose (RAC)<sup>16</sup>. Jia also mentioned that gel-like shape morphology as a consequence of losing crystallinity that shaping its initial fibrous shape. This report has a good agreement with our result in the cross-polarizer image of -20PALF50% that capturing no birefringence exists as evidence of amorphous cellulose was formed<sup>110</sup>. The gel-like shape was suggested relating to the phenomena that happen in forming RAC.

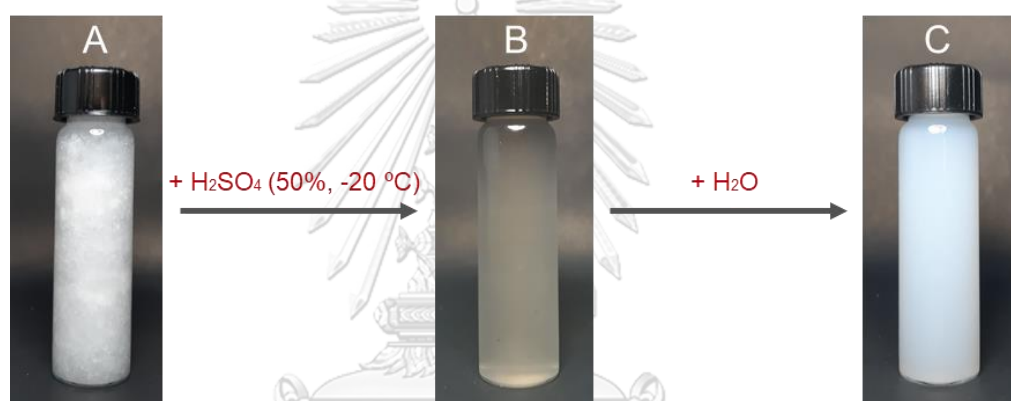


Figure 4.16 Transformation of (A) bleached PALF into (B) cellulose solution, then regenerate into (C) RAC after washed with DI water.

Figure 4.16 has recorded the transformation of bleached PALF into the RAC. The process of obtaining RAC started by adding cold 50% (v/v)  $\text{H}_2\text{SO}_4$  in bleached PALF. After 2 h continuously stirring in the ice bath, a transparent cellulose solution was obtained (Figure 4.16B). Then, DI water was used to wash the solution until pH reached  $\sim 7$ . After adding the DI water to the solution, it transformed into a solid gel-like solution (Figure 4.16C). The transparent cellulose solution has been explained in previous research by Huang et al. (2016). Huang explained that at low temperature ( $-20\text{ }^\circ\text{C}$ ), the process of hydrolysis when the hydronium ions ( $\text{H}_3\text{O}^+$ ) of  $\text{H}_2\text{SO}_4$  attached to the  $\beta$ -1,4-glycosidic bonds of cellulose that causing a split in the cellulose chain will be slowed. Because the hydrolysis happened slowly,  $\text{H}_3\text{O}^+$  and  $\text{SO}_4^{2-}$  broke down the inter and intramolecular H-bonding instead of breaking  $\beta$ -1,4-glycosidic bonds,

made the cellulose dissolved into a transparent cellulose solution, called as a dissolution process<sup>17</sup>. The reaction in this process has written in Figure 4.17 below.

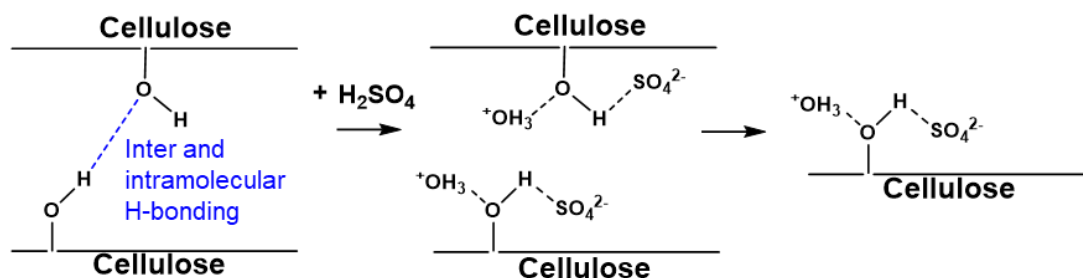


Figure 4.17 Chemical reaction of the dissolution process in cellulose<sup>111</sup>.

Cellulose dissolution in sulfuric acid involved a reaction between hydroxyl groups of cellulose and sulfuric acid to form cellulose sulfate (cellulose-O-SO<sub>4</sub>). Another by-reaction, such as acid hydrolysis of β-1,4-glycosidic bonds could occur, but the acid hydrolysis could be prevented by decreasing the dissolution temperature<sup>112</sup>. The washing process using DI water has formed a gel-like solution to remove acid from the system. The cellulose randomly tangled to each other after the acid leaving the structure, reconstructing the new H-bonding arrangement (regenerated process) but was not in an orderly arrangement like before the dissolution process. Since there was a reconstruction of a new arrangement in the structure, the transparent solution has transformed into a solid gel-like particle called regenerated amorphous cellulose (RAC)<sup>14, 16</sup>. The illustration has made to facilitate the understanding of PALF transformation into RAC (Figure 4.18).

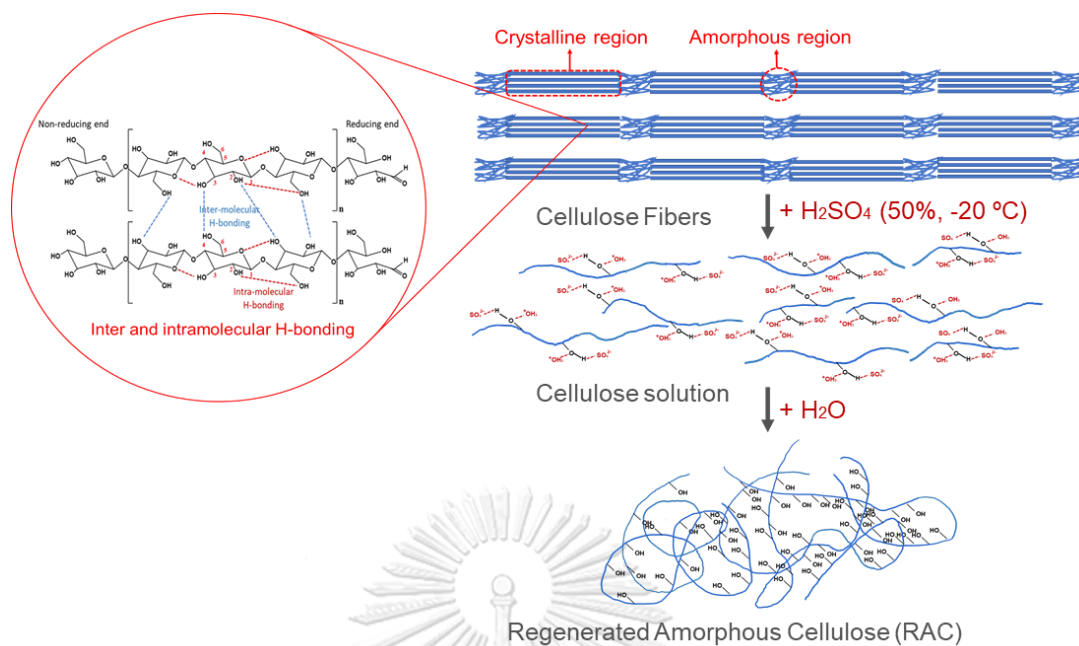


Figure 4.18 Drawing illustration of RAC transformation in 50% H<sub>2</sub>SO<sub>4</sub> at -20 °C.

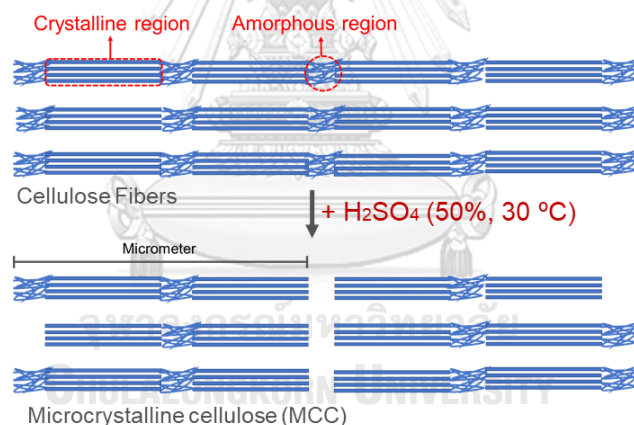


Figure 4.19 Partial hydrolysis occurred, forming microcrystalline cellulose (MCC).

However, the OM image of 30PALF50% in Figure 4.15C displayed the short fiber morphology with the length and width of  $37.63 \pm 14.19$  and  $3.85 \pm 0.66$   $\mu\text{m}$  categorized as microcrystalline cellulose (MCC)<sup>45</sup>. As we mentioned in the previous section, MCC was formed by partial hydrolysis. The acid randomly hydrolyzed cellulose by partially breaking the  $\beta$ -1,4-glycosidic, removing some amorphous regions, but some amorphous regions still remained attached in the structure, resulted in the microscale crystalline cellulose (Figure 4.19). Comparing with the MCC series in the previous section, it is worth noticing that the width in 30PALF50% is smaller

with the decrement of width ~33%, which means higher than in 25% H<sub>2</sub>SO<sub>4</sub> samples (~5-12.5%). This result suggested that acid concentration has a vital role in size reduction. The previous work of Du et al. (2016) mentioned that the hydrolysis severity is a critical factor of cellulose fibers size reduction<sup>113</sup>. By increasing the acid concentration, it will increase the severity of the reaction. The concentrated acid increased the hydrolysis effect in removing the amorphous region. It made the MCC length decreased until  $37.63 \pm 14.19 \mu\text{m}$  and defected more on the crystalline region due to stronger acid ability, reducing MCC's width.

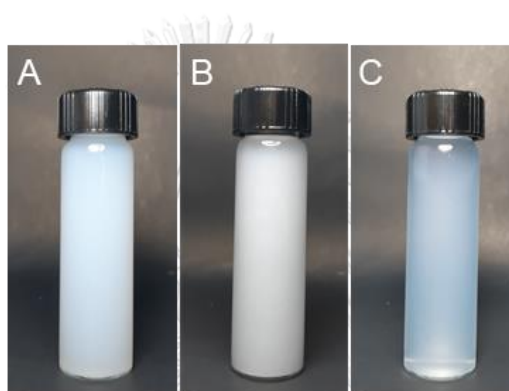


Figure 4.20 Photographic image of -20PALF50%, 30PALF50%, and 50PALF50%.

The morphology of 50PALF50% could not be seen in OM images (Figure 4.15D), assuming that the nanocrystalline cellulose (NCC) was formed because the OM could not capture the material with the size under  $1 \mu\text{m}$ <sup>114</sup>. Our assumption has been proven by the cross-polarizer image that exhibited a flow birefringence phenomenon, which is only shown in NCC. NCC alignment resulting in a structural anisotropy form and flow anisotropy exhibiting the flow birefringence phenomenon<sup>84</sup>. The presence of birefringence is also the evidence of the well-dispersed of NCC in water<sup>115</sup>. From this statement, we suggested that the physical appearance could also be an indicator of obtaining NCC because the physical appearance also relates to another characteristic of NCC. 50PALF50% performed a transparent homogeneous aqueous suspension and well-dispersed in the water (Figure 4.20C). These results have the same agreement with the NCC obtained from some previous works<sup>10, 52</sup>. NCC was transparent because NCC's size is so small in the nanometer scale<sup>116</sup>. The homogeneous and well-dispersed NCC came from the reaction between sulfuric acid and the surface hydroxyl

groups of NCC to yield negatively charged (surface) sulfate groups, promoting perfectly uniform dispersion nano rod-like in water<sup>42</sup>.

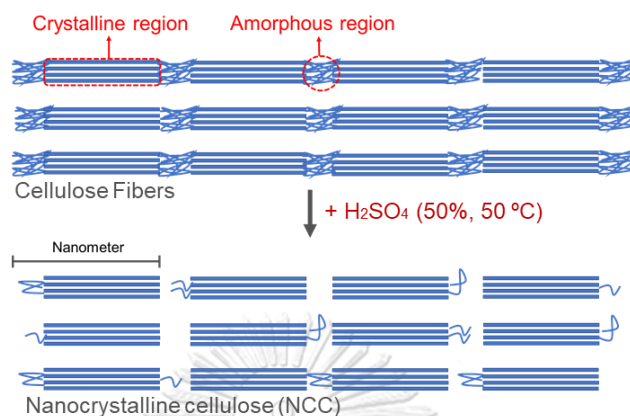


Figure 4.21 Drawing illustration of hydrolysis at 50 °C of 50% (v/v) H<sub>2</sub>SO<sub>4</sub>, forming nanocrystalline cellulose (NCC).

We have observed that obtaining NCC required an extreme condition to hydrolyzed the cellulose into a nanometer-scale of crystalline cellulose. This extreme condition referred to the high acid concentration (50% (v/v) H<sub>2</sub>SO<sub>4</sub>) at 50 °C. The extreme condition would help acid removed most of all amorphous regions, increased depolymerization, resulting in produced NCC<sup>41</sup>. The non-harsh condition of hydrolysis would lead to obtaining microcrystalline cellulose (MCC). The illustration has been made to explain the process of obtaining NCC (Figure 4.21).

#### 4.3.2 Chemical structural changes of PALF in 50% (v/v) H<sub>2</sub>SO<sub>4</sub>

FT-IR spectra have been taken to follow the chemical changes of RAC, MCC, and NCC that we obtained. Because of their complexity, FT-IR spectra were divided into two regions, which are the OH and CH stretching vibrations in the 3900–2700 cm<sup>-1</sup> region (Figure 4.22A) and the "fingerprint" region, which assigned to stretching vibrations of different groups of cellulose components at 1800–600 cm<sup>-1</sup> (Figure 4.22B). The corresponding band assignment has listed in Table 4.6.

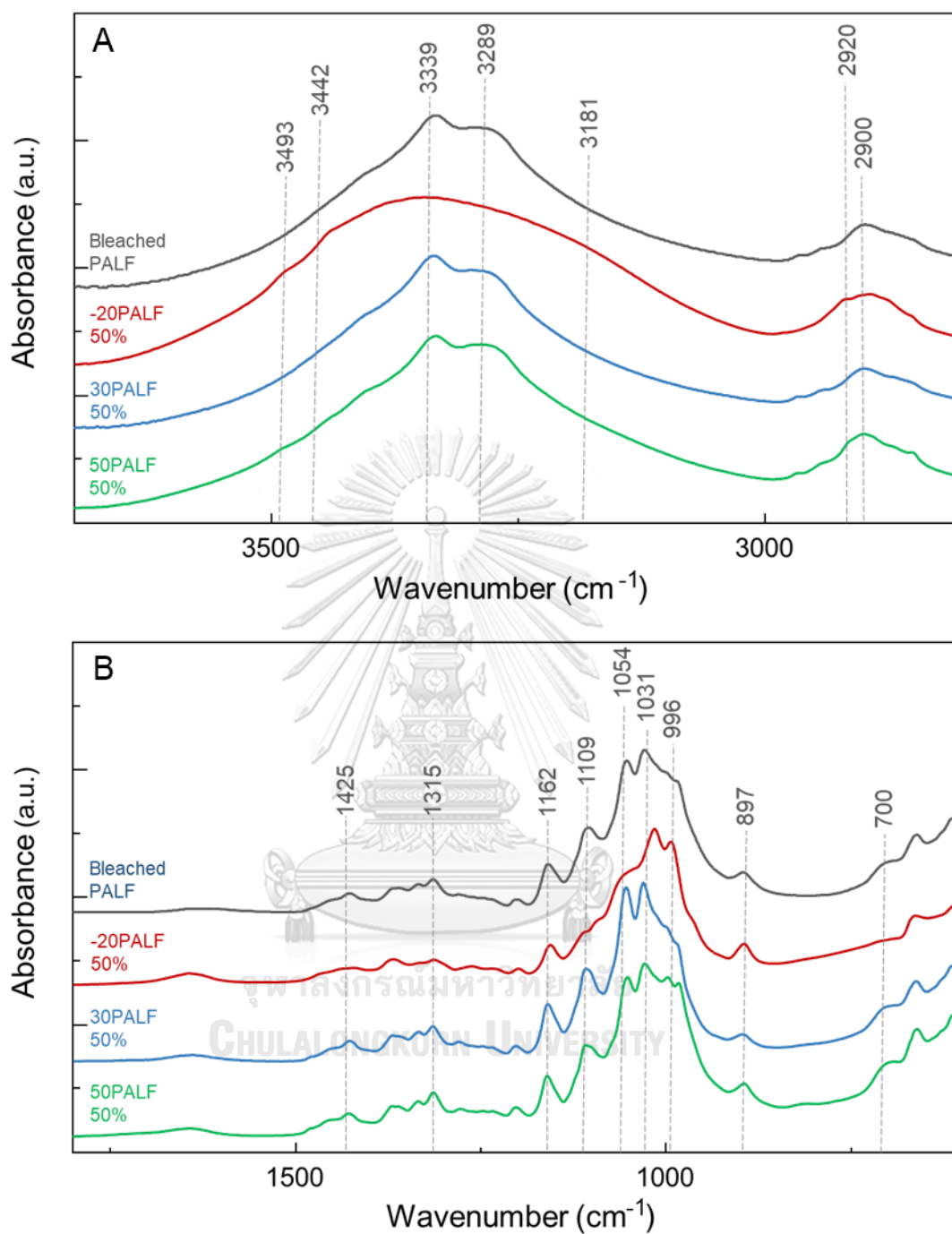


Figure 4.22 FT-IR spectra of bleached PALF, -20PALF50%, 30PALF50%, and 50PALF50% in the (A) 3900-2700 cm<sup>-1</sup> and (B) 1800-600 cm<sup>-1</sup> regions.

Table 4.6 Band assignment of FT-IR spectra from bleached PALF, -20PALF50%, 30PALF50%, 50PALF50%.

Wavenumber (cm <sup>-1</sup> )	Vibrational Mode	Band assignment	Reference
3493	$\gamma$ OH	OH stretching of weak H-bond	117
3442	$\gamma$ OH	OH stretching of intermolecular H-bonding at O(3)H $\cdots$ O'(6)H	117
3339	$\gamma$ OH	OH stretching of intramolecular H-bonding at O(3)H $\cdots$ O(5)	74-77
3289	$\gamma$ OH	OH stretching of intermolecular H-bonding at O(3)H $\cdots$ O'(6)H	77
3181		Unidentified H-bonds	117
1635		OH of water absorbed	74, 75, 81
1425	$\delta$ CH <sub>2</sub>	CH <sub>2</sub> scissoring of C(6)	74, 75, 78
1315	$\delta$ CH <sub>2</sub>	CH <sub>2</sub> wagging of C(6)	74, 78
1109		CO valence vibration of C(3)-O(3)H	74, 75
1054	$\gamma$ CO	CO stretching	74, 75
1031	$\gamma$ CO	CO stretching	74, 75, 81
996	$\gamma$ CO	CO stretching	74, 75, 81
897	$\gamma$ COC	C-O-C stretching asymmetric	16

Notes:  $\gamma$ : stretching,  $\delta$ : bending.

At -20PALF50%, the OH region (3900-3000 cm<sup>-1</sup>) corresponding to the inter and intramolecular H-bonding showed a different pattern compared to bleached PALF. This result suggested that there is arrangement changes in the inter and intramolecular H-bonding of the cellulose. The peak at 3493 cm<sup>-1</sup> correspondings to OH stretching of weak H-bonding, has appeared. The weak H-bonding has arisen due to the inter and intramolecular H-bonding broke down in the dissolution process. Then, in the regenerated process, they have arranged randomly and bonded weakly in the structure<sup>118</sup>. The peak at 3442 cm<sup>-1</sup> attributed to OH stretching of intermolecular H-bonding at O(3)H $\cdots$ O' (6)H possibly formed due to the new arrangement of H-bonding in RAC. The arrangement could not be capable of forming the same order H-bonding, making some H-bonding shifted. Peaks at 3339 and 3289 cm<sup>-1</sup> assigned to OH stretching of intramolecular H-bonding at O(3)H $\cdots$ O(5) and intermolecular H-bonding at O(3)H $\cdots$ O'(6)H, respectively. In the dissolution process, acid broke the

inter and intramolecular H-bonding of native cellulose resulted in their disappearance. These peaks also contribute to the gel-like shape that appeared in the OM image, showing the loss of ordered structure in the cellulose<sup>119</sup>. The shoulder peak at 3181  $\text{cm}^{-1}$  attributing to unidentified H-bonding has appeared only at -20PALF50%. Leng (2018) has reported that the peak at 3181  $\text{cm}^{-1}$  is the most unstable H-bonding and only appeared in amorphous cellulose. We proposed that it could have a connection with the appearance of peak 3493  $\text{cm}^{-1}$  proving that the new arrangement of H-bonding which is not strong, stable, or well-ordered.

In the 1800-600  $\text{cm}^{-1}$  region, there are also some changes in the FT-IR spectrum of -20PALF50%. At the peak at 1635  $\text{cm}^{-1}$  associating with OH of water absorbed from cellulose, it has the highest peak compared to other samples. This result indicated that -20PALF50% has the highest water absorption due to the amorphous structure. In the crystalline structure (MCC and NCC), water could not penetrate the cellulose well. In the amorphous form, it increased the capacity of the sample to hold into the water in consequence of disorder and weak H-bonding<sup>14, 120</sup>. Whereas the peak at 1425  $\text{cm}^{-1}$  ascribing to  $\text{CH}_2$  symmetric bending scissoring of C(6) has disappeared at -20PALF50%. This peak has been sensitive to the amount of crystalline. The absence of this peak indicating a significant decrease in its intensity reflected, reducing the degree of crystallinity of the sample<sup>16, 86</sup>. This peak has the same agreement with the cross-polarizer image, which showed no birefringence in the sample. The peak at 1315  $\text{cm}^{-1}$  associating with  $\text{CH}_2$  wagging of C(6) has lost in -20PALF50%. This peak is connected to the disappearance of the crystalline band (1425  $\text{cm}^{-1}$ ). The peak at 1109  $\text{cm}^{-1}$  representing CO valence vibration of C(3)-O(3)H has disappeared from -20PALF50%. The absence of this peak attributed to the disappearance of peaks at 3339 and 3289  $\text{cm}^{-1}$  that related to C(3)-O(3)H bonding. The peak at 1054 and  $\text{cm}^{-1}$  assigning to CO stretching has disappeared from the sample. Meanwhile, the new peak at 996  $\text{cm}^{-1}$  representing CO has appeared. These phenomena occurred due to the new arrangement in RAC. The peak at 897  $\text{cm}^{-1}$  designated as the amorphous absorption band and was more pronounced in -20PALF50%, suggesting the amorphous content was high<sup>16, 117</sup>.

On the other hand, FT-IR spectra of both 30PALF50% and 50PALF50% performed a similar pattern with bleached PALF. This result indicating that there is no

new arrangement has occurred. The hydrolysis did not change the arrangement of the chemical functional groups in MCC and NCC structure, only cutting the chain between cellulose at the  $\beta$ -1,4-glycosidic linkage.

### 4.3.3 X-ray diffraction patterns of bleached PALF and its cellulosic products

The X-ray diffractometer (XRD) was used to investigate the crystalline structure of samples. XRD patterns of bleached PALF, -20PALF50%, 30PALF50%, and 50PALF50% were displayed in Figure 4.23. The corresponding peak and crystallinity index (CI) have written in Table 4.7.

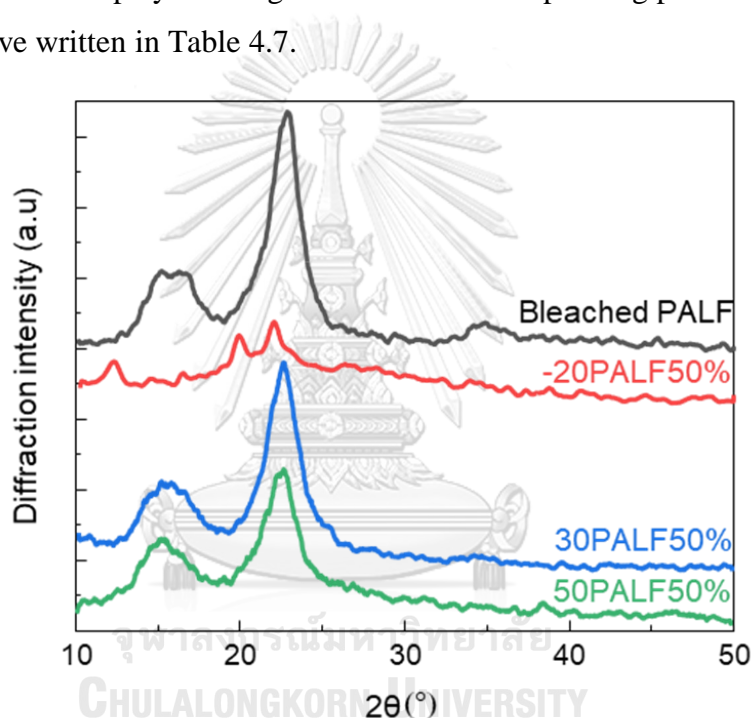


Figure 4.23 X-ray diffraction (XRD) patterns recorded from bleached PALF (black), -20PALF50% (red), 30PALF50% (blue), and 50PALF50% (green) samples.

Table 4.7 Corresponding peaks of XRD patterns and crystallinity index (CI).

Samples	$2\theta$ (°)		CI (%)
Bleached PALF	15.1	22.7	76.5
-20PALF50%	12.1	19.7	21.4
30PALF50%	15.1	22.7	74.6
50PALF50%	15.1	22.7	68.3

The XRD patterns of bleached PALF, 30PALF50%, and 50PALF50% exhibited a similar curve, showing peaks around  $2\theta = 15.1^\circ$  (1 -1 0) and  $22.7^\circ$  (2 0 0), attributing to cellulose I<sup>121</sup>. This result suggested that the crystal integrity of cellulose had been maintained in MCC and NCC<sup>122</sup>. However, -20PALF50% displayed a different pattern compared to other samples. The XRD pattern was almost flat, typical of regenerated amorphous cellulose (RAC), but showed off with three small peaks at  $12.1^\circ$  (1 -1 0),  $19.7^\circ$  (1 1 0), and  $21.4^\circ$  (2 0 0), corresponding to cellulose II<sup>56, 123</sup>. The small peaks of cellulose II were existed due to the storage of RAC in the aqueous condition. The aqueous condition might be happened to enhance arrangement of hydroxyl groups in RAC forming small amount cellulose II. Hattori et al. (2016) reported that even after obtained a fully amorphous product, the cellulose II would appear due to the storage in the aqueous condition.

The crystallinity index (CI) determined from these XRD curves were listed in Table 4.7. CI of bleached PALF, 30PALF50% and 50PALF50% were 76.5%, 74.6%, and 68.3%, respectively. In this research, we found that the decrement of crystallinity happened when the treatment temperature increased. The crystallinity decreased in 30PALF50% was about 1.9%, while in 50PALF50% was about 8.2%, compared to the bleached PALF, suggesting that the crystallinity decrement happened due to the defect of the crystalline region in the process of acid hydrolysis<sup>9, 51</sup>. The acid hydrolysis process removed the amorphous region but at the same time also slightly defected in the crystalline region. Das et al. (2017) also reported the decreasing of crystallinity about 3.7% in filter paper after the acid treatment<sup>51</sup>.

#### 4.3.4 Thermal properties of bleached PALF and cellulosic products

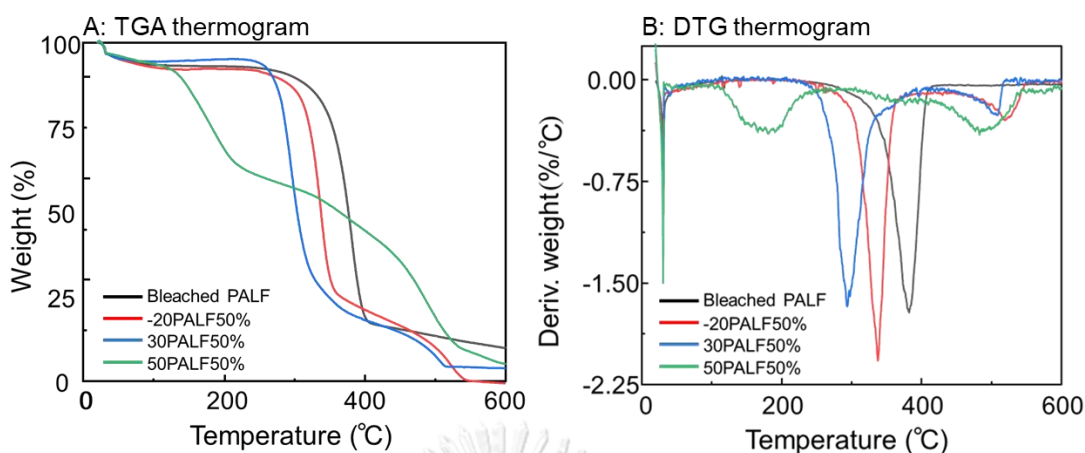


Figure 4.24 (A) TGA and (B) DTG thermograms of bleached PALF (black), -20PALF50% (red), 30PALF50% (blue), and 50PALF50% (green).

Table 4.8 Thermal properties profile of bleached PALF, -20PALF50%, 30PALF50%, and 50PALF50%.

Samples	Onset T (°C)	Decomposition T (°C)	Weight loss at 600 °C (%)
Bleached PALF	340	382	90.0
-20PALF50%	310	340	100.0
30PALF50%	272	293	96.0
50PALF50%	135	181	95.0

TGA and derived curves (DTG) were plotted as a function of temperature. An initial weight loss was observed for all samples upon heating to 100 °C. The weight loss corresponded to the vaporization and removal of moisture in the samples.<sup>124</sup>

Table 4.8 displayed the decrement of degradation temperature in -20PALF50%, 30PALF50%, and 50PALF50% compared to the bleached PALF due to the sulfate groups presence induced the decrease in degradation temperature<sup>21</sup>. For 30PALF50% (MCC), the behavior of the thermal properties is in the same agreement with the MCC obtained from 25% (v/v) H<sub>2</sub>SO<sub>4</sub> in the previous section. Meanwhile, thermographs of 50PALF50% revealed a remarkable decrement of the degradation temperature with a broad curve on the DTG thermograph. Some researchers have reported a similar decrement of degradation temperature in their NCC obtained from sulfuric acid

treatment<sup>12, 24, 87, 90</sup>. The high surface area of 50PALF50% (NCC) may play an essential role in this decrement of thermal properties<sup>102</sup>. The higher surface area would increase the access of more sulfate groups to attach to the cellulose surface. Sulfate groups would promote the degradation started faster and occurred in a broader temperature range, which explained the decrement phenomena and the broad curve at DTG thermograph<sup>108</sup>. In the case of 50PALF50%, degradation happened in two sub-processes. The first sub-process corresponds to the degradation of the more accessible regions, which are highly sulfated. The second sub-process corresponds to the crystalline fraction broke down that has not been attacked by sulfuric acid. These two sub-processes happened in a wide range of temperature degradation, causing a broad curve shaped<sup>87</sup>.

However, it is worth noticing that -20PALF50%, which is a RAC (310 °C), showed a higher onset temperature than MCC (272 °C) and NCC (135 °C), the crystalline products. We proposed that this is related to the arrangement of the RAC and the crystalline products. The amorphous cellulose arrangement was more accessible to the water and caused the sulfate groups to easier removed from the products. Meanwhile, crystalline products such as MCC and NCC were tightly packed by the well-ordered region results in the access of the water was limited<sup>125</sup>. FT-IR spectra of -20PALF50% also confirmed high water absorption (peak 1635 cm<sup>-1</sup>) in the amorphous cellulose. This result also supported by the previous work of Wang et al. (2007) that done repeated washing for more than one month, but small amounts of sulfate groups still remained in the NCC<sup>48</sup>.

## CHAPTER V

### CONCLUSIONS

In summary, the large scale production and economical purification of regenerated amorphous cellulose (RAC) have not been done. However, a simple process using sulfuric acid ( $\text{H}_2\text{SO}_4$ ) treatment has been developed to produce three types of cellulosic products from PALF, which are regenerated amorphous (RAC), microcrystalline (MCC), and nanocrystalline (NCC) cellulose. Temperature treatment and sulfuric acid concentration played an essential role in the cellulosic products that would obtain.  $\text{H}_2\text{SO}_4$  acid treatment has been done in 25% and 50% (v/v)  $\text{H}_2\text{SO}_4$  under three different temperatures (-20, 30, and 50 °C). In 25% (v/v)  $\text{H}_2\text{SO}_4$ , various MCC lengths (about  $29.57 \pm 9.99$  to  $106.40 \pm 61.10$   $\mu\text{m}$ ) were produced from different temperatures. Different temperatures in this condition gave the ability to control the MCC size without changing the chemical structure, confirmed by OM images and FT-IR spectra. Compared to the commercial MCC, Avicel PH101, MCC PALF obtained in this work offers definite advantages over Avicel PH101 regarding aspect ratio and uniformity. In 50% (v/v)  $\text{H}_2\text{SO}_4$ , three kinds of cellulosic products were obtained and could be differentiated using OM, cross-polarizer, FT-IR, and XRD characterizations. RAC was obtained at -20 °C, confirmed from the gel-like shape morphology, no birefringence shown, the crystalline band's disappearance at  $1425\text{ cm}^{-1}$  and increment of the amorphous band at  $897\text{ cm}^{-1}$  on FT-IR spectrum, and XRD patterns of amorphous cellulose with small peaks corresponding to cellulose II. MCC was obtained at 30 °C, showing a short fiber morphology in OM image with length and width at  $37.63 \pm 14.19$  and  $3.85 \pm 0.66$   $\mu\text{m}$ , respectively. NCC was obtained at 50 °C, showing flow birefringence phenomena, confirmed by cross-polarizer.

Furthermore, our MCC can be a potential alternative to produce a commercial MCC regarding well-defined aspect ratio and good uniformity. Producing RAC and NCC required adequate acid concentration and temperature treatment. By adjusting the temperature in an appropriate concentration, different products could be obtained.

## REFERENCES



จุฬาลงกรณ์มหาวิทยาลัย  
**CHULALONGKORN UNIVERSITY**

1. Jiang, Z.; Tang, L.; Gao, X.; Zhang, W.; Ma, J.; Zhang, L., Solvent regulation approach for preparing cellulose-nanocrystal-reinforced regenerated cellulose fibers and their properties. *ACS Omega* **2019**, *4* (1), 2001-2008.
2. Nuruddin, M.; Hosur, M.; Uddin, M. J.; Baah, D.; Jeelani, S., A novel approach for extracting cellulose nanofibers from lignocellulosic biomass by ball milling combined with chemical treatment. *Journal of Applied Polymer Science* **2016**, *133* (9), 42990.
3. Wang, S.; Lu, A.; Zhang, L., Recent advances in regenerated cellulose materials. *Progress in Polymer Science* **2016**, *53*, 169-206.
4. Choojit, S.; Ruengpeerakul, T.; Sangwichien, C., Optimization of acid hydrolysis of pineapple leaf residue and bioconversion to ethanol by *saccharomyces cerevisiae*. *Cellulose Chemistry and Technology* **2017**, *52* (3-4), 247-257.
5. Jirapornvaree, I.; Suppadit, T.; Popan, A., Use of pineapple waste for production of decomposable pots. *International Journal of Recycling of Organic Waste in Agriculture* **2017**, *6* (4), 345-350.
6. Maniruzzaman, M.; Rahman, M. A.; Gafur, M. A.; Fabritius, H.; Raabe, D., Modification of pineapple leaf fibers and graft copolymerization of acrylonitrile onto modified fibers. *Journal of Composite Materials* **2011**, *46* (1), 79-90.
7. Santos, R. M. d.; Flauzino Neto, W. P.; Silvério, H. A.; Martins, D. F.; Dantas, N. O.; Pasquini, D., Cellulose nanocrystals from pineapple leaf, a new approach for the reuse of this agro-waste. *Industrial Crops and Products* **2013**, *50*, 707-714.
8. Abraham, E.; Deepa, B.; Pothan, L. A.; Cintil, J.; Thomas, S.; John, M. J.; Anandjiwala, R.; Narine, S. S., Environmental friendly method for the extraction of coir fibre and isolation of nanofibre. *Carbohydrate Polymers* **2013**, *92* (2), 1477-83.
9. Kang, X.; Kuga, S.; Wang, C.; Zhao, Y.; Wu, M.; Huang, Y., Green preparation of cellulose nanocrystal and its application. *ACS Sustainable Chemistry & Engineering* **2018**, *6* (3), 2954-2960.

10. Wang, Z.; Yao, Z.; Zhou, J.; Zhang, Y., Reuse of waste cotton cloth for the extraction of cellulose nanocrystals. *Carbohydrate Polymers* **2017**, *157*, 945-952.
11. Wang, H.; Zuo, M.; Ding, N.; Yan, G.; Zeng, X.; Tang, X.; Sun, Y.; Lei, T.; Lin, L., Preparation of nanocellulose with high-pressure homogenization from pretreated biomass with cooking with active oxygen and solid alkali. *ACS Sustainable Chemistry & Engineering* **2019**, *7* (10), 9378-9386.
12. Oliveira, F. B. d.; Bras, J.; Pimenta, M. T. B.; Curvelo, A. A. d. S.; Belgacem, M. N., Production of cellulose nanocrystals from sugarcane bagasse fibers and pith. *Industrial Crops and Products* **2016**, *93*, 48-57.
13. Cheng, M.; Qin, Z.; Chen, Y.; Hu, S.; Ren, Z.; Zhu, M., Efficient extraction of cellulose nanocrystals through hydrochloric acid hydrolysis catalyzed by inorganic chlorides under hydrothermal conditions. *ACS Sustainable Chemistry & Engineering* **2017**, *5* (6), 4656-4664.
14. Hashaikeh, R.; Abushammala, H., Acid mediated networked cellulose: Preparation and characterization. *Carbohydrate Polymers* **2011**, *83* (3), 1088-1094.
15. Chang, C.; Peng, J.; Zhang, L.; Pang, D.-W., Strongly fluorescent hydrogels with quantum dots embedded in cellulose matrices. *Journal of Materials Chemistry* **2009**, *19* (41).
16. Jia, X.; Chen, Y.; Shi, C.; Ye, Y.; Wang, P.; Zeng, X.; Wu, T., Preparation and characterization of cellulose regenerated from phosphoric acid. *Journal of Agricultural Food and Chemistry* **2013**, *61* (50), 12405-14.
17. Huang, W.; Wang, Y.; Zhang, L.; Chen, L., Rapid dissolution of spruce cellulose in H<sub>2</sub>SO<sub>4</sub> aqueous solution at low temperature. *Cellulose* **2016**, *23* (6), 3463-3473.
18. Singhsa, P.; Narain, R.; Manuspiya, H., Bacterial cellulose nanocrystals (bcnc) preparation and characterization from three bacterial cellulose sources and development of functionalized bcncs as nucleic acid delivery systems. *ACS Applied Nano Materials* **2017**, *1* (1), 209-221.

19. Cherian, B. M.; Leão, A. L.; de Souza, S. F.; Thomas, S.; Pothan, L. A.; Kottaisamy, M., Isolation of nanocellulose from pineapple leaf fibres by steam explosion. *Carbohydrate Polymers* **2010**, *81* (3), 720-725.
20. Asim, M.; Abdan, K.; Jawaid, M.; Nasir, M.; Dashtizadeh, Z.; Ishak, M.R.; Hoque, M.E., A review on pineapple leaves fibre and its composites. *International Journal of Polymer Science* **2015**, 950567.
21. Johar, N.; Ahmad, I.; Dufresne, A., Extraction, preparation and characterization of cellulose fibres and nanocrystals from rice husk. *Industrial Crops and Products* **2012**, *37* (1), 93-99.
22. Lee, H. V.; Hamid, S. B.; Zain, S. K., Conversion of lignocellulosic biomass to nanocellulose: structure and chemical process. *Scientific World Journal* **2014**, 631013.
23. Flauzino Neto, W. P.; Silvério, H. A.; Dantas, N. O.; Pasquini, D., Extraction and characterization of cellulose nanocrystals from agro-industrial residue – Soy hulls. *Industrial Crops and Products* **2013**, *42*, 480-488.
24. Kargarzadeh, H.; Ahmad, I.; Abdullah, I.; Dufresne, A.; Zainudin, S. Y.; Sheltami, R. M., Effects of hydrolysis conditions on the morphology, crystallinity, and thermal stability of cellulose nanocrystals extracted from kenaf bast fibers. *Cellulose* **2012**, *19* (3), 855-866.
25. Sritrakul, N.; Nitisinprasert, S.; Keawsompong, S., Evaluation of dilute acid pretreatment for bioethanol fermentation from sugarcane bagasse pith. *Agriculture and natural resources* **2017**, *51* (6), 512-519.
26. Kucharska, K.; Rybarczyk, P.; Holowacz, I.; Lukajtis, R.; Glinka, M.; Kaminski, M., Pretreatment of lignocellulosic materials as substrates for fermentation processes. *Molecules* **2018**, *23* (11).
27. Talebi Amiri, M.; Bertella, S.; Questell-Santiago, Y. M.; Luterbacher, J. S., Establishing lignin structure-upgradeability relationships using quantitative (1)H-(13)C heteronuclear single quantum coherence nuclear magnetic resonance (HSQC-NMR) spectroscopy. *Chemical Science* **2019**, *10* (35), 8135-8142.
28. Mancera, A.; Fierro, V.; Pizzi, A.; Dumarçay, S.; Gérardin, P.; Velásquez, J.; Quintana, G.; Celzard, A., Physicochemical characterisation of sugar cane

- bagasse lignin oxidized by hydrogen peroxide. *Polymer Degradation and Stability* **2010**, 95 (4), 470-476.
29. Schoenherr, S.; Ebrahimi, M.; Czermak, P., *Lignin degradation processes and the purification of valuable products. in Lignin - trends and applications* **2018**.
  30. Harmsen, P.; Huijgen, W.; Bermudez, L.; Bakker, R., *Literature review of physical and chemical pretreatment processes for lignocellulosic biomass*. Wageningen UR Food & Biobased Research, **2010**.
  31. Zhang, J.; Choi, Y. S.; Yoo, C. G.; Kim, T. H.; Brown, R. C.; Shanks, B. H., Cellulose–Hemicellulose and Cellulose–Lignin Interactions during Fast Pyrolysis. *ACS Sustainable Chemistry & Engineering* **2015**, 3 (2), 293-301.
  32. Giudicianni, P.; Cardone, G.; Ragucci, R., Cellulose, hemicellulose and lignin slow steam pyrolysis: Thermal decomposition of biomass components mixtures. *Journal of Analytical and Applied Pyrolysis* **2013**, 100, 213-222.
  33. Karimi, K.; Taherzadeh, M. J., A critical review of analytical methods in pretreatment of lignocelluloses: Composition, imaging, and crystallinity. *Bioresource Technology* **2016**, 200, 1008-18.
  34. Zhao, X.; Cheng, K.; Liu, D., Organosolv pretreatment of lignocellulosic biomass for enzymatic hydrolysis. *Applied Microbiology and Biotechnology* **2009**, 82 (5), 815-27.
  35. Inoue, H.; Yano, S.; Endo, T.; Sakaki, T.; Sawayama, S., Combining hot-compressed water and ball milling pretreatments to improve the efficiency of the enzymatic hydrolysis of eucalyptus. *Biotechnology for Biofuels* **2008**, 1 (1), 2.
  36. Tan, H.; Yang, R.; Sun, W.; Wang, S., Peroxide–acetic acid pretreatment to remove bagasse lignin prior to enzymatic hydrolysis. *Industrial & Engineering Chemistry Research* **2010**, 49 (4), 1473-1479.
  37. Martino, D. C.; Colodette, J. L.; Chandra, R.; Saddler, J., Steam explosion pretreatment used to remove hemicellulose to enhance the production of a eucalyptus organosolv dissolving pulp. *Wood Science and Technology* **2017**, 51 (3), 557-569.
  38. Oushabi, A.; Sair, S.; Oudrhiri Hassani, F.; Abboud, Y.; Tanane, O.; El Bouari, A., The effect of alkali treatment on mechanical, morphological and thermal properties of date palm fibers (DPFs): Study of the interface of DPF–

- Polyurethane composite. *South African Journal of Chemical Engineering* **2017**, *23*, 116-123.
39. Mussatto, S. I.; Rocha, G. J. M.; Roberto, I. C., Hydrogen peroxide bleaching of cellulose pulps obtained from brewer's spent grain. *Cellulose* **2008**, *15* (4), 641-649.
  40. Moon, R. J.; Martini, A.; Nairn, J.; Simonsen, J.; Youngblood, J., Cellulose nanomaterials review: structure, properties and nanocomposites. *Chemical Society Reviews* **2011**, *40* (7), 3941-94.
  41. Trache, D.; Hussin, M. H.; Haafiz, M. K.; Thakur, V. K., Recent progress in cellulose nanocrystals: sources and production. *Nanoscale* **2017**, *9* (5), 1763-1786.
  42. Habibi, Y.; Lucia, L. A.; Rojas, O. J., Cellulose nanocrystals: chemistry, self-assembly, and applications. *Chemical Reviews* **2010**, *110* (6), 3479-3500.
  43. Trache, D.; Donnot, A.; Khimeche, K.; Benelmir, R.; Brosse, N., Physico-chemical properties and thermal stability of microcrystalline cellulose isolated from Alfa fibres. *Carbohydrate Polymers* **2014**, *104*, 223-30.
  44. Samir, M. A. A.; Alloin, F.; Dufresne, A., Review of recent research into cellulosic whiskers, their properties and their application in nanocomposite field. *Biomacromolecules* **2005**, *6*, 612-626.
  45. Thoorens, G.; Krier, F.; Leclercq, B.; Carlin, B.; Evrard, B., Microcrystalline cellulose, a direct compression binder in a quality by design environment--a review. *International Journal of Pharmaceutics* **2014**, *473* (1-2), 64-72.
  46. Flauzino Neto, W. P.; Putaux, J.-L.; Mariano, M.; Ogawa, Y.; Otaguro, H.; Pasquini, D.; Dufresne, A., Comprehensive morphological and structural investigation of cellulose I and II nanocrystals prepared by sulphuric acid hydrolysis. *RSC Advances* **2016**, *6* (79), 76017-76027.
  47. George, J.; Sabapathi, S. N., Cellulose nanocrystals: synthesis, functional properties, and applications. *Nanotechnology Science and Applications* **2015**, *8*, 45-54.
  48. Wang, N.; Ding, E.; Cheng, R., Thermal degradation behaviors of spherical cellulose nanocrystals with sulfate groups. *Polymer* **2007**, *48* (12), 3486-3493.

49. Jiang, M.; Seney, R.; Bayliss, P. C.; Kitchens, C. L., Carbon nanotube and cellulose nanocrystal hybrid films. *Molecules* **2019**, *24* (14).
50. Kalashnikova, I.; Bizot, H.; Cathala, B.; Capron, I., New Pickering emulsions stabilized by bacterial cellulose nanocrystals. *Langmuir* **2011**, *27* (12), 7471-9.
51. Das, K.; Ray, D.; Bandyopadhyay, N. R.; Sengupta, S., Study of the properties of microcrystalline cellulose particles from different renewable resources by XRD, FTIR, Nanoindentation, TGA and SEM. *Journal of Polymers and the Environment* **2010**, *18* (3), 355-363.
52. Balakrishnan, P.; Gopi, S.; Geethamma, V. G.; Kalarikkal, N.; Thomas, S., Cellulose nanofiber vs nanocrystals from pineapple leaf fiber: a comparative studies on reinforcing efficiency on starch nanocomposites. *Macromolecular Symposia* **2018**, *380* (1).
53. Uddin, K. M. A.; Jokinen, V.; Jahangiri, F.; Franssila, S.; Rojas, O. J.; Tuukkanen, S., Disposable microfluidic sensor based on nanocellulose for glucose detection. *Global Challenges* **2019**, *3* (2).
54. Gu, R.; Yun, H.; Chen, L.; Wang, Q.; Huang, X., Regenerated cellulose films with amino-terminated hyperbranched polyamic anchored nanosilver for active food packaging. *ACS Applied Bio Materials* **2019**, *3* (1), 602-610.
55. Cao, Y.; Li, H.; Zhang, Y.; Zhang, J.; He, J., Structure and properties of novel regenerated cellulose films prepared from cornhusk cellulose in room temperature ionic liquids. *Journal of Applied Polymer Science* **2010**, *116* (1), 547-554.
56. Hattori, K.; Arai, A., Preparation and hydrolysis of water-stable amorphous cellulose. *ACS Sustainable Chemistry & Engineering* **2016**, *4* (3), 1180-1186.
57. Pinkert, A.; Marsh, K.N.; Pang, S.; Staiger, M.P., Ionic liquids and their interaction with cellulose. *Chemical Reviews* **2009**, *109*, 6712-6728.
58. Tan, X.; Chen, L.; Li, X.; Xie, F., Effect of anti-solvents on the characteristics of regenerated cellulose from 1-ethyl-3-methylimidazolium acetate ionic liquid. *International Journal of Biological Macromolecules* **2019**, *124*, 314-320.
59. Iguchi, M.; Aida, T. M.; Watanabe, M.; Smith, R. L., Jr., Dissolution and recovery of cellulose from 1-butyl-3-methylimidazolium chloride in presence of water. *Carbohydrate Polymers* **2013**, *92* (1), 651-8.

60. Cai, J.; Zhang, L.; Liu, S.; Liu, Y.; Xu, X.; Chen, X.; Chu, B.; Guo, X.; Xu, J.; Cheng, H., Dynamic self-assembly induced rapid dissolution of cellulose at low temperatures. *Macromolecules* **2008**, *41*, 9345–9351.
61. Dupont, A.-L., Cellulose in lithium chloride/N,N-dimethylacetamide, optimisation of a dissolution method using paper substrates and stability of the solutions. *Polymer* **2003**, *44* (15), 4117-4126.
62. Qi, H.; Liu, J.; Gao, S.; Mäder, E., Multifunctional films composed of carbon nanotubes and cellulose regenerated from alkaline–urea solution. *Journal of Materials Chemistry A* **2013**, *1* (6), 2161-2168.
63. Zhang, B. X.; Azuma, J.-i.; Uyama, H., Preparation and characterization of a transparent amorphous cellulose film. *RSC Advances* **2015**, *5* (4), 2900-2907.
64. Segal, L., Creely, J.J., Martin Jr., A.E., Conrad, C.M., An empirical method for estimating the degree of crystallinity of native cellulose using the X-ray diffractometer. *Textile Research Journal* **1959**, *29*, 9.
65. Hossain, M. A.; Phung, T. K.; Rahaman, M. S.; Tulaphol, S.; Jasinski, J. B.; Sathitsuksanoh, N., Catalytic cleavage of the  $\beta$ -O-4 aryl ether bonds of lignin model compounds by Ru/C catalyst. *Applied Catalysis A: General* **2019**, 582.
66. Weinstock I.A.; Atalla, R.H.; Reiner, R.S.; Moen, M.A.; Hammel, K.E.; Houtman, C.J.; Hill, C.L., A new environmentally benign technology and approach to bleaching kraft pulp. Polyoxometalates for selective delignification and waste mineralization. *New Journal of Chemistry* **1996**, *20*: 269–275.
67. Agbor, V. B.; Cicek, N.; Sparling, R.; Berlin, A.; Levin, D. B., Biomass pretreatment: fundamentals toward application. *Biotechnology Advances* **2011**, *29* (6), 675-85.
68. Kumar, A. K.; Sharma, S., Recent updates on different methods of pretreatment of lignocellulosic feedstocks: a review. *Bioresources and Bioprocessing* **2017**, *4* (1), 7.
69. Derkacheva, O.; Sukhov, D., Investigation of lignins by FTIR spectroscopy. *Macromolecular Symposia* **2008**, *265* (1), 61-68.
70. Rahmawati, N.; Ohashi, Y.; Honda, Y.; Kuwahara, M.; Fackler, K.; Messner, K.; Watanabe, T., Pulp bleaching by hydrogen peroxide activated with copper

- 2,2'-dipyridylamine and 4-aminopyridine complexes. *Chemical Engineering Journal* **2005**, *112* (1-3), 167-171.
71. Brooks, R.E.; Moore, S.B., Alkaline hydrogen peroxide bleaching of cellulose. *Cellulose* **2000**, *7*, 263–286.
72. He, W.; Gao, W.; Fatehi, P., Oxidation of kraft lignin with hydrogen peroxide and its application as a dispersant for kaolin suspensions. *ACS Sustainable Chemistry & Engineering* **2017**, *5* (11), 10597-10605.
73. Kadla, J. F.; Chang, H.; Jameel, H.; The reactions of lignins with hydrogen peroxide at high temperature. *Holzforschung* **1997**, *51*, 428-434.
74. Carrillo, F.; Colom, X.; Suñol, J. J.; Saurina, J., Structural FTIR analysis and thermal characterisation of lyocell and viscose-type fibres. *European Polymer Journal* **2004**, *40* (9), 2229-2234.
75. Haule, L. V.; Carr, C. M.; Rigout, M., Investigation into the supramolecular properties of fibres regenerated from cotton based waste garments. *Carbohydrate Polymers* **2016**, *144*, 131-9.
76. Moriana, R.; Vilaplana, F.; Ek, M., Cellulose nanocrystals from forest residues as reinforcing agents for composites: a study from macro- to nano-dimensions. *Carbohydrate Polymers* **2016**, *139*, 139-49.
77. Fareez, I. M.; Ibrahim, N. A.; Wan Yaacob, W. M. H.; Mamat Razali, N. A.; Jasni, A. H.; Abdul Aziz, F., Characteristics of cellulose extracted from Josapine pineapple leaf fibre after alkali treatment followed by extensive bleaching. *Cellulose* **2018**, *25* (8), 4407-4421.
78. Lionetto, F.; Del Sole, R.; Cannoletta, D.; Vasapollo, G.; Maffezzoli, A., monitoring wood degradation during weathering by cellulose crystallinity. *Materials* **2012**, *5* (10), 1910-1922.
79. Alawar, A.; Hamed, A. M.; Al-Kaabi, K., Characterization of treated date palm tree fiber as composite reinforcement. *Composites Part B: Engineering* **2009**, *40* (7), 601-606.
80. Braga, R. M.; Queiroga, T. S.; Calixto, G. Q.; Almeida, H. N.; Melo, D. M.; Melo, M. A.; Freitas, J. C.; Curbelo, F. D., The energetic characterization of pineapple crown leaves. *Environmental Science Pollution Research* **2015**, *22* (23), 18987-93.

81. Oh, S. Y.; Yoo, D. I.; Shin, Y.; Kim, H. C.; Kim, H. Y.; Chung, Y. S.; Park, W. H.; Youk, J. H., Crystalline structure analysis of cellulose treated with sodium hydroxide and carbon dioxide by means of X-ray diffraction and FTIR spectroscopy. *Carbohydrate Research* **2005**, *340* (15), 2376-91.
82. Poletto, M.; Zattera, A. J.; Santana, R. M. C., Structural differences between wood species: Evidence from chemical composition, FTIR spectroscopy, and thermogravimetric analysis. *Journal of Applied Polymer Science* **2012**, *126* (S1), E337-E344.
83. Zhou, Y.; Stuart-Williams, H.; Farquhar, G. D.; Hocart, C. H., The use of natural abundance stable isotopic ratios to indicate the presence of oxygen-containing chemical linkages between cellulose and lignin in plant cell walls. *Phytochemistry* **2010**, *71* (8-9), 982-93.
84. Mtibe, A.; Liganiso, L. Z.; Mathew, A. P.; Oksman, K.; John, M. J.; Anandjiwala, R. D., A comparative study on properties of micro and nanopapers produced from cellulose and cellulose nanofibres. *Carbohydrate Polymers* **2015**, *118*, 1-8.
85. Atalla, R. H.; VanderHart, D. L., Native cellulose: A composite of two distinct crystalline forms. *Science* **1984**, *223*, 283-285.
86. Lee, C. M.; Mohamed, N. M.; Watts, H. D.; Kubicki, J. D.; Kim, S. H., Sum-frequency-generation vibration spectroscopy and density functional theory calculations with dispersion corrections (DFT-D2) for cellulose Ialpha and Ibeta. *Journal of Physical Chemistry B* **2013**, *117* (22), 6681-92.
87. Martínez-Sanz, M.; Lopez-Rubio, A.; Lagaron, J. M., Optimization of the nanofabrication by acid hydrolysis of bacterial cellulose nanowhiskers. *Carbohydrate Polymers* **2011**, *85* (1), 228-236.
88. Yu, H.; Qin, Z.; Liang, B.; Liu, N.; Zhou, Z.; Chen, L., Facile extraction of thermally stable cellulose nanocrystals with a high yield of 93% through hydrochloric acid hydrolysis under hydrothermal conditions. *Journal of Materials Chemistry A* **2013**, *1* (12).
89. Makarem, M.; Lee, C. M.; Kafle, K.; Huang, S.; Chae, I.; Yang, H.; Kubicki, J. D.; Kim, S. H., Probing cellulose structures with vibrational spectroscopy. *Cellulose* **2019**, *26* (1), 35-79.

90. Vasconcelos, N. F.; Feitosa, J. P.; da Gama, F. M.; Morais, J. P.; Andrade, F. K.; de Souza Filho, M. S.; Rosa, M. F., Bacterial cellulose nanocrystals produced under different hydrolysis conditions: Properties and morphological features. *Carbohydrate Polymers* **2017**, *155*, 425-431.
91. Carrier, M.; Auret, L.; Bridgwater, A.; Knoetze, J. H., Using apparent activation energy as a reactivity criterion for biomass pyrolysis. *Energy & Fuels* **2016**, *30* (10), 7834-7841.
92. Zhou, L.; Hui, H.; Can, J.; Li, M.; Peng, Y., Cellulose nanocrystals from cotton stalk for reinforcement of poly(vinyl alcohol) composites. *Cellulose Chemistry And Technology* **2017**, *51* (1-2), 109-119.
93. Kim, H.-S.; Kim, S.; Kim, H.-J.; Yang, H.-S., Thermal properties of bio-flour-filled polyolefin composites with different compatibilizing agent type and content. *Thermochimica Acta* **2006**, *451* (1-2), 181-188.
94. Thygesen, A.; Oddershede, J.; Lilholt, H.; Thomsen, A. B.; Ståhl, K., On the determination of crystallinity and cellulose content in plant fibres. *Cellulose* **2005**, *12* (6), 563-576.
95. Zhu, C.; Richardson, R. M.; Potter, K. D.; Koutsomitopoulou, A. F.; van Duijneveldt, J. S.; Vincent, S. R.; Wanasekara, N. D.; Eichhorn, S. J.; Rahatekar, S. S., High modulus regenerated cellulose fibers spun from a low molecular weight microcrystalline cellulose solution. *ACS Sustainable Chemistry & Engineering* **2016**, *4* (9), 4545-4553.
96. Prado, K. S.; Spinace, M. A. S., Isolation and characterization of cellulose nanocrystals from pineapple crown waste and their potential uses. *International Journal of Biological Macromolecules* **2019**, *122*, 410-416.
97. Trache, D.; Hussin, M. H.; Hui Chuin, C. T.; Sabar, S.; Fazita, M. R.; Taiwo, O. F.; Hassan, T. M.; Haafiz, M. K., Microcrystalline cellulose: Isolation, characterization and bio-composites application-A review. *International Journal of Biological Macromolecules* **2016**, *93* (Pt A), 789-804.
98. Vehovec, T.; Gartner, A.; Planinsek, O.; Obreza, A., Influence of different types of commercially available microcrystalline cellulose on degradation of perindopril erbumine and enalapril maleate in binary mixtures. *Acta Pharmaceutica* **2012**, *62* (4), 515-28.

99. Dong, X.M.; Revol J.F.; Gray, D.G., Effect of microcrystallite preparation conditions on the formation of colloid crystals of cellulose. *Cellulose* **1998**, *5* (1),19-32.
100. Kupiainen, L.; Ahola, J.; Tanskanen, J., Distinct effect of formic and sulfuric acids on cellulose hydrolysis at high temperature. *Industrial & Engineering Chemistry Research* **2012**, *51* (8), 3295-3300.
101. Ioelovich, M., Optimal conditions for isolation of nanocrystalline cellulose particles. *Nanoscience and Nanotechnology* **2012**, *2* (2), 9-13.
102. Tan, X. Y.; Abd Hamid, S. B.; Lai, C. W., Preparation of high crystallinity cellulose nanocrystals (CNCs) by ionic liquid solvolysis. *Biomass and Bioenergy* **2015**, *81*, 584-591.
103. Keshk, S. M. A. S.; Haija, M. A., A new method for producing microcrystalline cellulose from *Gluconacetobacter xylinus* and kenaf. *Carbohydrate Polymers* **2011**, *84* (4), 1301-1305.
104. Chaerunisaa, A.Y.; Sriwidodo, S.; Abdassah, M., *Microcrystalline cellulose as pharmaceutical excipient. In pharmaceutical formulation design - recent practices* **2019**.
105. Xiong, R.; Zhang, X.; Tian, D.; Zhou, Z.; Lu, C., Comparing microcrystalline with spherical nanocrystalline cellulose from waste cotton fabrics. *Cellulose* **2012**, *19* (4), 1189-1198.
106. Ruan, D.; Huang, Q.; Zhang, L., Structure and properties of Cds/regenerated cellulose nanocomposites. *Macromolecular Materials and Engineering* **2005**, *290* (10), 1017-1024.
107. Araki, J.; Wada, M.; Kuga, S.; Okano, T., Flow properties of microcrystalline cellulose suspension prepared by acid treatment of native cellulose. *Colloids Surface A* **1998**, *142* (1), 75–82.
108. Roman, M.; Winter, W.T.; Effect of sulfate groups from sulfuric acid hydrolysis on the thermal degradation behavior of bacterial cellulose. *Biomacromolecules* **2004**, *5*, 1671–1677.
109. Kumar, V.; Reus-Medina, M.; Yang, D., Preparation, characterization, and tableting properties of a new cellulose-based pharmaceutical aid. *International Journal of Pharmaceutics* **2002**, *235*, 129–140.

110. Deguchi, S.; Tsujii, K.; Horikoshi, K., Crystalline-to-amorphous transformation of cellulose in hot and compressed water and its implications for hydrothermal conversion. *Green Chemistry*. **2008**, *10* (2), 191-196.
111. Feng, L.; Chen, Z.-l., Research progress on dissolution and functional modification of cellulose in ionic liquids. *Journal of Molecular Liquids* **2008**, *142* (1-3), 1-5.
112. Zhang, Y.-H. P.; Cui, J.; Lynd, L. R.; Kuang, L. R. A., Transition from cellulose swelling to cellulose dissolution by o-phosphoric acid: Evidence from enzymatic hydrolysis and supramolecular structure. *Biomacromolecules* **2006**, *7*, 644–648.
113. Du, H.; Liu, C.; Mu, X.; Gong, W.; Lv, D.; Hong, Y.; Si, C.; Li, B., Preparation and characterization of thermally stable cellulose nanocrystals via a sustainable approach of FeCl<sub>3</sub>-catalyzed formic acid hydrolysis. *Cellulose* **2016**, *23* (4), 2389-2407.
114. Liu, Y.; Wang, H.; Yu, G.; Yu, Q.; Li, B.; Mu, X., A novel approach for the preparation of nanocrystalline cellulose by using phosphotungstic acid. *Carbohydr Polym* **2014**, *110*, 415-22.
115. Silvério, H. A.; Flauzino Neto, W. P.; Dantas, N. O.; Pasquini, D., Extraction and characterization of cellulose nanocrystals from corncob for application as reinforcing agent in nanocomposites. *Industrial Crops and Products* **2013**, *44*, 427-436.
116. Klemm, D.; Kramer, F.; Moritz, S.; Lindstrom, T.; Ankerfors, M.; Gray, D.; Dorris, A., Nanocelluloses: a new family of nature-based materials. *Angewandte Chemie International Edition in English* **2011**, *50* (24), 5438-66.
117. Leng, E.; Zhang, Y.; Peng, Y.; Gong, X.; Mao, M.; Li, X.; Yu, Y., In situ structural changes of crystalline and amorphous cellulose during slow pyrolysis at low temperatures. *Fuel* **2018**, *216*, 313-321.
118. Marechal, Y.; Chanzy, H., The hydrogen bond network in I<sub>β</sub> cellulose as observed by infrared spectrometry. *Journal of Molecular Structure* **2000**, *523*, 183–196.
119. Lu, R.; Zhang, X.; Fu, L.; Wang, H.; Briber, R. M.; Wang, H., Amorphous cellulose thin films. *Cellulose* **2020**, *27* (6), 2959-2965.

120. Abidi, N.; Manike, M., X-ray diffraction and FTIR investigations of cellulose deposition during cotton fiber development. *Textile Research Journal* **2017**, *88* (7), 719-730.
121. French, A. D., Idealized powder diffraction patterns for cellulose polymorphs. *Cellulose* **2013**, *21* (2), 885-896.
122. Chen, W.; Yu, H.; Liu, Y.; Hai, Y.; Zhang, M.; Chen, P., Isolation and characterization of cellulose nanofibers from four plant cellulose fibers using a chemical-ultrasonic process. *Cellulose* **2011**, *18* (2), 433-442.
123. Henrique, M. A.; Flauzino Neto, W. P.; Silvério, H. A.; Martins, D. F.; Gurgel, L. V. A.; Barud, H. d. S.; Morais, L. C. d.; Pasquini, D., Kinetic study of the thermal decomposition of cellulose nanocrystals with different polymorphs, cellulose I and II, extracted from different sources and using different types of acids. *Industrial Crops and Products* **2015**, *76*, 128-140.
124. Mandal, A.; Chakrabarty, D., Isolation of nanocellulose from waste sugarcane bagasse (SCB) and its characterization. *Carbohydrate Polymers* **2011**, *86* (3), 1291-1299.
125. Kontturi, E.; Suchy, M.; Penttila, P.; Jean, B.; Pirkkalainen, K.; Torkkeli, M.; Serimaa, R., Amorphous characteristics of an ultrathin cellulose film. *Biomacromolecules* **2011**, *12* (3), 770-7.

## VITA

**NAME** Gisma Coraima Asmarani

**DATE OF BIRTH** 16 April 1995

**PLACE OF BIRTH** Trenggalek, Indonesia

**INSTITUTIONS ATTENDED** Gadjah Mada University

**HOME ADDRESS** SK charoenpol apartment 557/3 Banthatong Rd., Wangmai, Pathumwan, Bangkok 10330

**PUBLICATION** Gisma Coraima Asmarani, Umphan Ngoensawat, Attasith Parnsubsakul, Sanong Ekgasit, Effect of Temperature on the Cellulosic Products from Sulfuric-acid-treated Pineapple Leaf Fiber, Proceeding of The Pure and Applied Chemistry International Conference 2020 (PACCON 2020), February 13-14, 2020, IMPACT Forum, Muangthong Thani, Bangkok, Thailand.